nature COMMUNICATIONS

ARTICLE

Received 24 Nov 2014 | Accepted 15 May 2015 | Published 14 Jul 2015

DOI: 10.1038/ncomms8537 OPEN

Climate-induced variations in global wildfire danger from 1979 to 2013

W. Matt Jolly[1], Mark A. Cochrane[2], Patrick H. Freeborn[1,2], Zachary A. Holden[3], Timothy J. Brown[4], Grant J. Williamson[5] & David M.J.S. Bowman[5]

Climate strongly influences global wildfire activity, and recent wildfire surges may signal fire weather-induced pyrogeographic shifts. Here we use three daily global climate data sets and three fire danger indices to develop a simple annual metric of fire weather season length, and map spatio-temporal trends from 1979 to 2013. We show that fire weather seasons have lengthened across 29.6 million km^2 (25.3%) of the Earth's vegetated surface, resulting in an 18.7% increase in global mean fire weather season length. We also show a doubling (108.1% increase) of global burnable area affected by long fire weather seasons (>1.0 σ above the historical mean) and an increased global frequency of long fire weather seasons across 62.4 million km^2 (53.4%) during the second half of the study period. If these fire weather changes are coupled with ignition sources and available fuel, they could markedly impact global ecosystems, societies, economies and climate.

[1] US Forest Service, Rocky Mountain Research Station, Fire Sciences Laboratory, 5775 Highway 10 West, Missoula, Montana 59803, USA. [2] Geospatial Sciences Center of Excellence (GSCE), South Dakota State University, 1021 Medary Avenue, Wecota Hall, Box 506B, Brookings, South Dakota 57007, USA. [3] US Forest Service Region 1, 200 East Broadway Street, Missoula, Montana 59802, USA. [4] Desert Research Institute (DRI), Western Regional Climate Center, 2215 Raggio Parkway, Reno, Nevada 89512-1095, USA. [5] School of Biological Sciences, The University of Tasmania, Private Bag 55, Hobart, Tasmania 7001, Australia. Correspondence and requests for materials should be addressed to W.M.J. (email: mjolly@fs.fed.us).

Wildfires play a pivotal, dynamic role in terrestrial and atmospheric systems[1]. Global annual burned area estimates approach 350 MHa per year[2], and annual pyrogenic CO_2 emissions can exceed 50% of fossil fuel combustion emissions[3–5]. Fires play an essential ecological role in flammable ecosystems: some are managed to clear forests, promote grazing and establish plants[6], while others are suppressed to protect human lives and property, regardless of how they ignite. Recently, there has been a surge of extremely destructive fires with corresponding social disruptions and substantial economic costs. Over the last decade, annual wildfire suppression costs on US federal lands exceeded $1.7B US dollars[7] and $1B US dollars in Canada[8]. When all components are considered, including preparedness/suppression costs and economic losses, these total costs are substantially higher. In Australia in 2005, total wildfire costs were estimated at nearly $9.4B US dollars or 1.3% of their Gross Domestic Product[9]. Therefore, the driving factors of contemporary wildfire activity changes must be understood to ensure that wildfires are effectively managed to promote healthy ecosystems while minimizing negative socio-economic impacts.

Wildfires occur at the intersection of dry weather, available fuel and ignition sources[10]. Weather is the most variable and largest driver of regional burned area[11–14]. Temperature, relative humidity, precipitation and wind speed independently influence wildland fire spread rates and intensities, and the alignment of multiple weather extremes, such as the co-occurrence of hot, dry and windy conditions leads to the most severe fires[15]. Global temperatures have increased by $\sim$0.2 °C per decade over the last three decades[16], possibly leading to an acceleration of the global water cycle with more intense rainfall events[17], more severe and widespread droughts[18] (despite drought frequencies appearing unchanged[19]) and regional humidity variations[20]. Regional droughts are also tightly coupled to sea surface temperature variations[21], and regional water availability variations can explain a significant proportion of the variations in burned area[22]. Climatic changes are implicated in global fire variations[23] and are expected to increase fire season severity over the coming decades[24]. While several studies have examined climate-induced regional and circumboreal trends in fire danger[25–30], a comprehensive global assessment of the interactions of recent climatic changes that lead to an expansion or contraction of fire seasons is lacking.

Landscape-scale fire behaviour is determined by local weather conditions, but biome-level wildfire potential is more appropriately associated with fire danger indices, which are representative of daily synoptic weather patterns[11]. Independent fire danger indices have been developed and applied for different regions worldwide. All are based on daily surface weather variables that are related to the ignitability, spread rate and the control difficulty of an initiating wildland fire[31] and they are closely related to the magnitude and extent of fire activity[32,33]. Furthermore, these indices capture changes in fuel (live and dead plant material) moistures, and thus scale to fuel consumption[34] and pyrogenic emission production[5].

Here we present an analysis of daily global fire weather trends from 1979 to 2013 based on three sub-daily global meteorological data sets (the National Center for Environmental Prediction (NCEP) Reanalysis, NCEP-DOE Reanalysis II and the European Centre for Medium-Range Weather Forecasts (ECMWF) Interim Reanalysis)[35–37] between $\sim$0.75° and 2.0° grid cell resolution. We use these data to calculate the US Burning Index[38], the Canadian Fire Weather Index[39] and the Australian (or McArthur) Forest Fire Danger Index[40]. Daily fire danger indices (normalized to a common scale and resampled to a common resolution) were used to derive a fire weather season length, defined as the number of days each year when fire danger is above half its value range, for each year in each grid cell using a technique commonly used to determine growing season length from satellite-derived vegetation indices[41,42]. Because climate studies using multi-model ensembles are generally superior to single model approaches[43], all nine fire weather season lengths for each location were averaged into an ensemble mean fire weather season length, hereafter referred to as 'Fire Weather Season Length' (See Supplementary Methods). This metric was examined to identify global and regional patterns in fire weather season length changes as well as changes in the frequency of, and the area affected by, long fire weather seasons (defined as $>1.0\ \sigma$ above historical mean) over the last 35 years.

Results

Global fire weather trends. Ensemble mean annual maximum temperature across the vegetated land surface increased by 0.184 °C per decade from 1979 to 2013 (Supplementary Table 1). This global trend is comparable to the global land temperature trends reported by the Intergovernmental Panel on Climate Change of 0.268, 0.315, 0.188 and 0.203 K per decade[4]. Mean annual global vegetated surface maximum temperature was significantly correlated to the Goddard Institute of Space Studies (GISS) land-surface temperature anomalies ($\rho = 0.88$, $P < 0.001$)[16]. The amount of area witnessing unusually hot years, where maximum temperature was more than 1 s.d. from the mean, also showed a significant increase of 6.3% per decade (Supplementary Table 1). Mean annual minimum relative humidity showed a weak but significant trend of -0.127% per decade but showed no significant changes in affected area. There were no significant trends in mean annual total precipitation or total precipitation affected area but we did observe a significant increase in mean annual rain-free days, where the mean number of dry days increased by 1.31 days per decade and the global area affected by anomalously dry years significantly increased by 1.6% per decade. Despite an absence of global trends in some key meteorological variables, there were distinct regional annual climate trends and changes in anomalous weather event affected area frequency (Fig. 1).

Global fire weather season length trends. Even more distinct patterns and trends in annual climate anomalies emerged when the meteorological data were used to calculate fire danger indices and then combined into metrics characterizing the fire weather season length and long fire weather season affected areas. Globally, fire weather season length increased by 18.7% from 1979 to 2013 (Fig. 2a), with statistically significant increases observed across 25.3% (29.6 M km^2) of the global vegetated area and decreases in only 10.7% (12.5 M km^2) (Fig. 3a). Long fire weather season affected area, defined as the total global area observing fire weather seasons >1 s.d. from the mean, has increased by 3.1% per year from 1979 to 2013, leading to a 108.1% increase in global long fire weather season affected area (Fig. 2b). The frequency of long fire weather seasons increased across 53.4% of the global vegetated area (62.4M km^2) as observed between 1996 and 2013, compared with 1979–1996, with decreased frequency only observed across 34.6% (40.4 M km^2) (Fig. 3b). Since 1979, there have been 6 years, all in the last decade, where >20% of the global vegetated area has been affected by long fire weather seasons (2005, 2007, 2009, 2010, 2012 and 2013). Both fire weather season metrics were strongly correlated with the global mean annual number of days without wetting rainfall (>0.1 mm) (Fig. 2c), where global mean rain-free days accounted for 49.7% of the variation in global fire weather season length and 33.8% of the variation in global long fire weather season affected area.

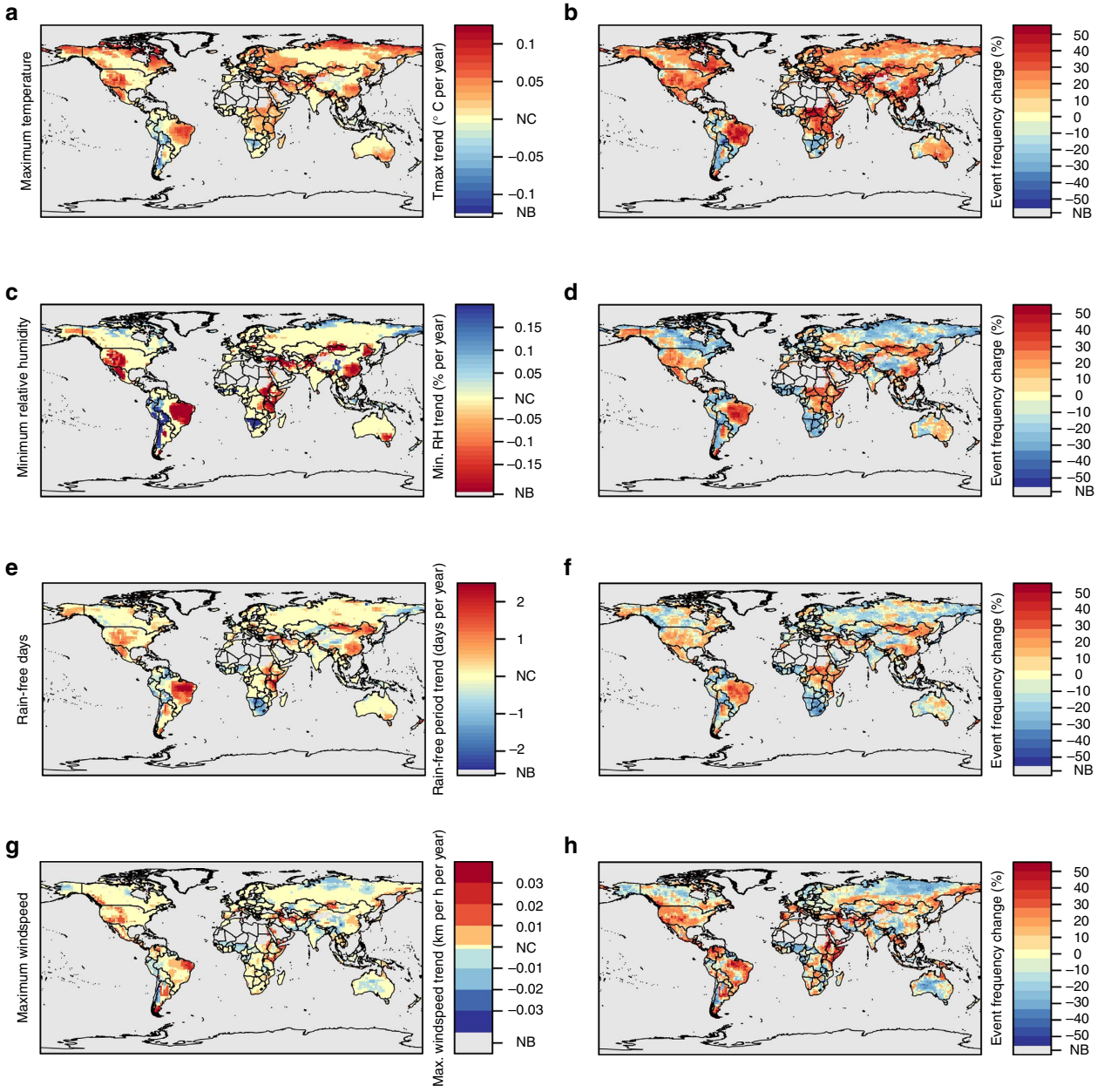

Figure 1 | Long-term trends and changes in anomalous event frequency of maximum temperature, minimum relative humidity, annual rain-free days and maximum wind speed. a,**c**,**e**,and,**g** show areas with significant trends in annual fire weather variables. **b**,**d**,**f** and **h** show the change in frequency of the number of years with anomalous mean annual weather conditions ($>1\sigma$ above historical mean) from 1996 to 2013 compared with the number of anomalies observed from 1979 to 1996. Areas with little or no burnable vegetation are shown in grey (NB) and NC indicates areas with no significant change. Red areas indicate locations where fire weather conditions are becoming increasingly more severe or anomalously severe weather events are becoming more frequent, while blue areas indicate locations where climatic influences on fire potential are lessening or weather events are becoming less frequent.

Annual fire weather season length anomaly maps for a subset of known severe fire years are presented in Fig. 4 and anomalies for all years are presented in Supplementary Figs 1–4 and annual ensemble-mean anomaly data are available as Supplementary Data 1.

Fire weather season length and long fire weather season affected area increased significantly across all continents except Australia (Table 1). Globally, most biomes showed significant increases in fire weather season metrics with the exceptions of temperate and montane grasslands, savannas and shrublands and boreal forests/taiga and tundra (Table 2). The strongest trends were observed in tropical and subtropical grasslands, savannas and shrublands. Continent × biome trends indicate that regional variations in fire weather season metrics were much stronger than global trends (Table 3).

Comparisons to country-wide reported burned area. Inter-annual variations in mean US fire weather season length were significantly correlated with variation in annual burned area reported by the US National Interagency Fire Center[44] over the full time series from 1979 to 2013 and also from 1992 to 2013, when fire occurrence data quality was highest[45] ($\rho = 0.679$ and 0.683, respectively, $P < 0.001$). Further, long fire weather season

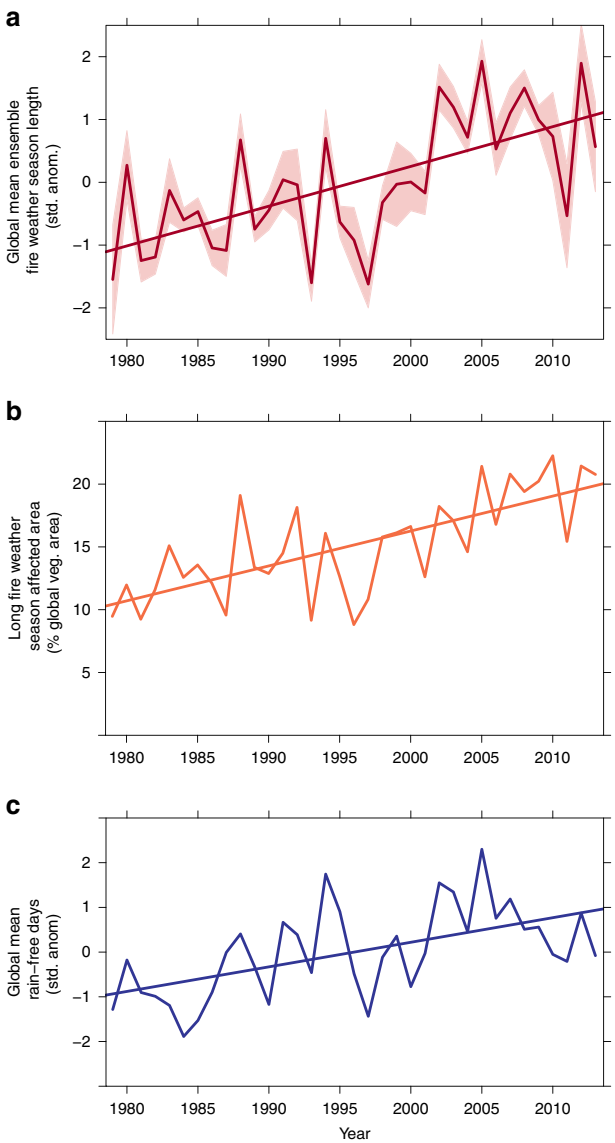

Figure 2 | Trends in global fire weather season length metrics and rain-free days. (**a**) Changes in the global mean fire weather season length from 1979 to 2013 with 95% confidence limits between ensemble members (shaded area). (**b**) Total global annual area affected by long fire weather seasons ($>1\sigma$ of historical mean). (**c**) Inter-annual variations in the standard anomalies of global mean rain-free days. Global mean rain-free days accounted for 49.7% of the variation in global fire weather season length and 33.8% of the variation in global long fire weather season affected area.

affected area was also significantly correlated to the burnt area variations of the full and limited time series ($\rho = 0.663$ and 0.715, respectively, $P < 0.001$) (Table 4 and Supplementary Fig. 5). Inter-annual variations in mean fire weather season length were also significantly correlated to inter-annual burned area variations from 1980 to 2013 across Spain, Portugal, France, Italy, Greece and Latvia (Table 4), and inter-annual variations in long fire weather season affected area were significantly correlated with burned area for Spain, Portugal, Italy and Latvia (Table 4 and Supplementary Figs 6–8). Both mean fire weather season length and long fire weather season affected area, constrained to only boreal forests where most Canadian fires occur, were only weakly correlated to burned area across Canadian forests ($\rho = 0.3$ and 0.324, respectively, $P < 0.1$) (Table 4 and Supplementary Fig. 5).

Comparisons to global land carbon uptake. Variation in fire danger metrics have been shown to be closely related to fuel consumption[34], and fire activity is generally inversely correlated with vegetation productivity[47]. Likewise, fire weather season length and long fire weather season affected area were significantly correlated with global net land carbon flux calculated from an analysis of the global carbon budget from 1979 to 2012 (ref. 48) (See Supplementary Methods) ($\rho = -0.38$ and $\rho = -0.48$, $n = 33$, $P < 0.05$ and $P < 0.01$, respectively, Supplementary Fig. 9). In addition, when correlations were constrained to the time period that satellite burned area observations were available from the Moderate Resolution Imaging Spectroradiometer (MODIS) (2001-2012), and thus where estimates of land-use change carbon emissions were more certain[2], correlations between fire weather season length, long fire season affected area and net land carbon fluxes increased substantially to $\rho = -0.797$ and $\rho = -0.825$, respectively, $n = 12$, $P < 0.01$). The highest correlations between the net land carbon flux and continental biome mean fire weather season metrics were observed in the tropical and subtropical forests, grasslands and savannas and xeric shrublands of South America where regional fire weather season length metrics accounted for between 15.7 and 29.7% of the variations in global net land carbon flux (Table 5).

Discussion

Fire weather season length and long fire weather season affected area significantly increased across all vegetated continents except Australia. For example, significant fire weather season lengthening has occurred throughout much of Africa, particularly the subtropical grasslands and savannas of the eastern half of the continent (Fig. 3) and across Africa's Mediterranean forests, woodlands and scrub. Persistent fire weather season length increases in ecosystems such as South Africa's Mediterranean fynbos could lead to more frequent severe burning conditions and more area burned, shortening fire return intervals and threatening these biodiversity-rich shrublands[49]. Recent climatic changes have mitigated wildland fire potential in some regions of Africa since 1979. For example, drought during the early 1980s (ref. 50) lengthened fire weather seasons in the West African subtropics. Drought conditions have subsequently subsided, leading to a steady contraction of the fire weather season lengths across much of West Africa (Fig. 3).

Our ensemble fire weather season length metric captured important wildfire events throughout Eurasia such as the Indonesian fires of 1997–98 where peat fires, following an El Niño-induced drought, released carbon equivalent to 13–40% of the global fossil fuel emissions from only 1.4% of the global vegetated land area (Fig. 4, 1997–1998)[46] and the heatwave over Western Russia in 2010 (Fig. 4, 2010) that led to its worst fire season in recorded history and triggered extreme air pollution in Moscow[51]. Our metric also revealed similar impacts across Eastern Canada in 2010, where high temperatures and significant water deficits led to large wildfires (Fig. 4, 2010)[52]. European Mediterranean forests were also identified as being susceptible to significant changes: the inner-quartile range of fire weather season length trends indicate a lengthening of 12 to 19 days, with a maximum increase of nearly a month (29 days) from 1979 to 2013 (Table 6). This is consistent with a lengthening of the fire weather season in Spain during 2012 (Fig. 4, 2012) where fires burned more area than any year in the previous decade[49].

Over the last several decades, the US has witnessed a marked increase in large wildfire frequency and duration with the greatest increases observed in the temperate coniferous forests of the Northern Rocky Mountains[53,54]. These trends are widely attributed to shifts towards earlier snowmelt timing[54], though

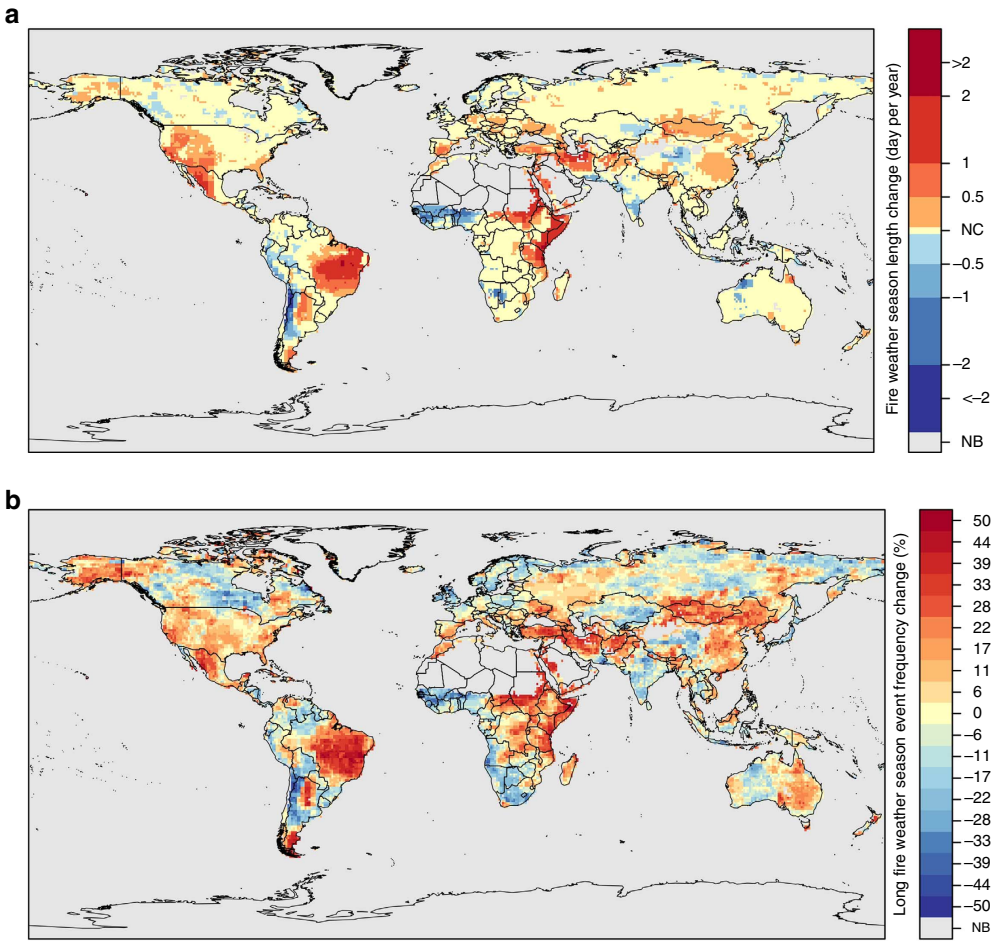

Figure 3 | Global patterns of fire weather season length changes from 1979 to 2013. a shows areas with significant trends in fire weather season length from 1979 to 2013. **b** shows regions that have experienced changes in the frequency of long fire weather seasons ($>1\sigma$ above historical mean) during the second half of the study period (1996–2013) compared with the number of events observed during the first half (1979–1996). Areas with little or no burnable vegetation are shown in grey (NB) and NC indicates areas with no significant change. Reds indicate areas where fire weather seasons have lengthened or long fire weather seasons have become more frequent. Blues indicate areas where fire weather seasons have shortened or long fire weather seasons have become less frequent.

fire activity in the desert Southwest has also been attributed to warming-driven increases in vapour pressure deficit[55] and variability in the timing of spring precipitation[56]. Our results extend these findings by demonstrating that areas with the most significant change in fire weather season length occur where not only temperature but also changes in humidity, length of rain-free intervals and wind speeds are most pronounced. In 2012, for example, longer-than-normal fire weather seasons across an unprecedented 47.4% of the vegetated area of the US (Fig. 4, 2012) culminated in a near-record setting ~3.8 MHa of burned area. In addition, our results show significant fire weather season lengthening throughout much of the Eastern US Coastal Plains. Over the last decade, this region has witnessed a marked uptick in wildfires and a group of large fires in Okefenokee National Wildlife Refuge, the Osceola National Forest and adjacent lands burned ~243 KHa in 2007 (ref. 57), one of those fires ranked as the twelfth largest fire in the US history.

Fire weather season length and long fire weather season affected area were only weakly correlated to Canadian boreal forest burned area (Table 4). This may be caused by averaging across the large zonal and meridional climatic gradients across the country. Future work should examine relationships between provincial fire activity and fire weather season metrics. In addition, our fire weather season length metric captures variations in the number of days each year that fires are likely to burn, but it does not account for inter-annual variations in fire season severity. Further work should consider both a lengthening fire season and an increase in within-season fire weather severity as causal mechanisms of burned area variations.

South America's tropical and subtropical forests, grasslands and savannas have experienced tremendous fire weather season length changes, with a median increase of 33 days over the last 35 years (Fig. 3a and Table 6). Our metric captured a rare drought in the Amazon in 2005 that prompted long fire weather seasons, leading to a dramatic increase in basin-wide fire activity[58] (Fig. 4, 2005). Longer fire seasons prolong conducive burning conditions, potentially expanding areas susceptible to escaped deforestation fires[59] and subsequently strengthening feedbacks in regional climate-fire dynamics[60].

In contrast to all other continents in our analysis, Australia showed no significant trends in biome-level fire season length, but we identified regional increases in the frequency of anomalously long fire weather seasons, especially from 1996 to 2013 (Fig. 3b). Our analysis also captures climatic droughts that contributed to the Ash Wednesday fires in Victoria (1983) (Fig. 4, 1982–1983), the Canberra bushfires (2003) (Supplementary Fig. 3), the Black

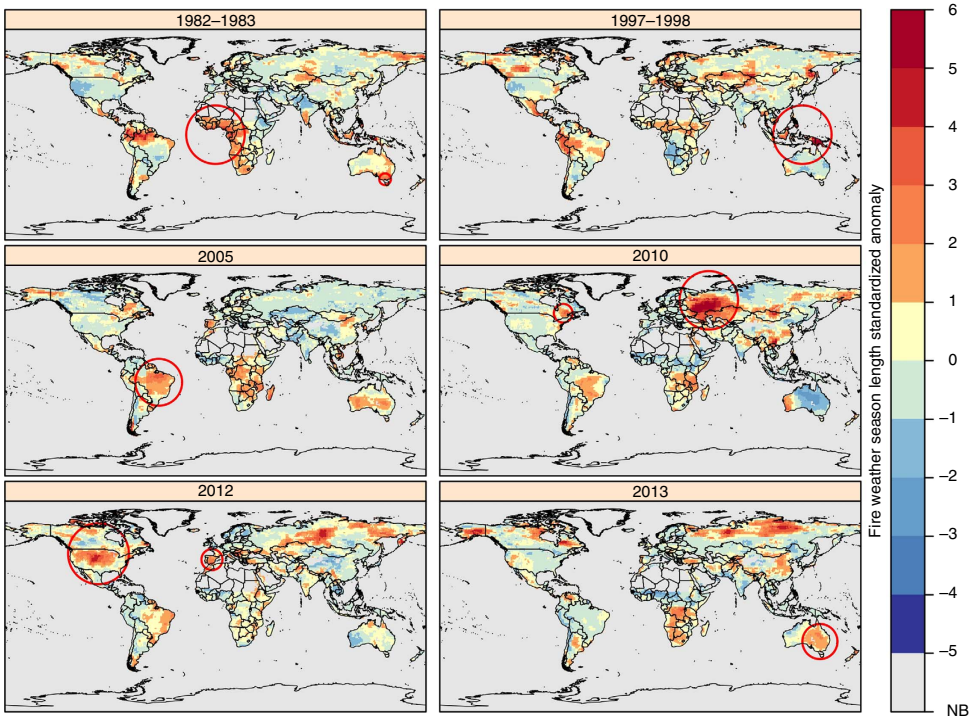

Figure 4 | Examples of fire weather season length standardized anomalies during significant global fire events. Red colours indicate areas where fire weather season anomalies are >1 s.d. from the mean, while blue areas indicate shorter-than-normal fire weather season lengths. Areas with little or no burnable vegetation are shown in grey (NB). Red circles denote regions with significant fire activity during that time period. El Niño periods often span multiple calendar years (for example, 1982–1983), so in these cases, the maximum anomaly of either year was mapped above. Maps of all years (1979–2013) are included as Supplementary Figs 1–4.

Table 1 | Continental trends in fire weather season length and long fire weather season affected area.

Continent	Mean fire weather season length trend (days per year)	Long fire weather season affected area trend (% glob. veg. area per year)
Africa	0.1542**	NS
Eurasia	0.0475***	0.0973***
Australia/New Zealand	NS	NS
North America	0.1519***	0.0726**
South America	0.2249**	0.0545**

NS, not significant.
Results of non-parametric tests examining temporal trends in the continental-mean fire weather season length and long fire weather season affected area from 1979 to 2013. (***$P<0.01$, **$P<0.05$, *$P<0.1$). Slopes were estimated using the Theil–Sen non-parametric trend slope estimator and significance tests were performed using the Mann–Kendall trend test following a four-step approach to reduce the effects of serial autocorrelation on significance tests[66].

Saturday fires (2009) (Supplementary Fig. 4) and the widespread heatwave across Australia in the summer of 2012–2013 that promoted long fire weather seasons and intense bushfire activity across most of the Eastern half of the country (Fig. 4, 2013). Australian fires seasons are dominated by periods of benign weather followed by years with extreme fire weather conditions. Such high inter-annual variability reflects climate modes, such as the El Niño Southern Oscillation (ENSO) and the Indian Ocean Dipole, which can heavily influence inter-annual rainfall variations and subsequently affect wildfire potential throughout Australia[61,62].

Fire weather season length imperfectly scales with actual fire activity because fires may not be ignited, there may be no available fuel, or they may be suppressed by humans. Nonetheless, our global fire weather season length metrics were significantly correlated to global net land carbon flux. These correlations were negative, suggesting that when average fire weather seasons are longer-than-normal or when long seasons impacted more global burnable area, net global terrestrial carbon uptake is reduced. Generally, low correlations between fire weather season length and global land carbon uptake are to be expected because wildfires represent a small proportion of the total land carbon flux. However, if our fire season metrics were combined with other metrics of global land carbon uptake that have been produced by others[63,64], they may improve our ability to assess the cumulative impacts of climatic changes on terrestrial carbon fluxes. Correlations between global net land carbon flux and continental-scale, biome mean fire weather season length metrics were highest across South American tropical and subtropical forests, savannas and grasslands and xeric shrublands (Table 5), highlighting that the strongest coupling between fire weather and global carbon emissions is occurring in an area of intense land-use pressure.

Global fire regimes are the combined results of available fuel, ignition sources and conducive fire weather[10]. As such, leveraging well-established fire danger indices to explore changes in global wildfire weather only capture part of the potential variations in global pyrogeography. Regionally, our documented fire weather changes may not appreciably alter fire regimes if fires are not ignited or if there is no fuel. However, we observed an overall lengthening of the number of days each year that wildfires may burn across more than a quarter of the Earth's vegetated surface and these fire weather changes could manifest themselves as a

Table 2 | Global biome trends in fire weather season length and long fire weather season affected area.

Biome	Mean fire weather season length trend (days per year)	Long fire weather season affected area trend (% glob. veg. area per year)
Tropical forests	0.089**	NS
Temperate broadleaf and mixed forests	0.103***	0.0464***
Temperate conifer forests	0.184***	0.0150***
Tropical and subtropical grasslands, savannas and shrublands	0.220***	0.06278**
Temperate and montane grasslands, savannas and shrublands	NS	0.0255**
Boreal forests/taiga and tundra	NS	NS
Mediterranean forests, woodlands and scrub	0.159**	0.0105***
Xeric shrublands	0.151***	0.0535***

NS, not significant.
Results of non-parametric tests examining temporal trends in the biome mean fire weather season length and long fire weather season affected area. (***$P<0.01$, **$P<0.05$, *$P<0.1$). Slopes were estimated using the Theil–Sen non-parametric trend slope estimator and significance tests were performed using the Mann–Kendall trend test following a four-step approach to reduce the effects of serial autocorrelation on significance tests[66].

Table 3 | Continental × biome trends in fire weather season length and long fire weather season affected area.

Continent	Biome	Mean fire weather season length (EFWSL) trend (days per year)	Long fire weather season affected area (ALFWS) affected area trend (% area per year)
Africa	Tropical forest	0.1321**	NS
	Tropical and subtropical grasslands, savannas and shrublands	0.1899**	0.3181*
	Temperate and montane grasslands, savannas and shrublands	NS	NS
	Mediterranean forests, woodlands and scrub	0.2292**	0.5642*
	Xeric shrublands	NS	NS
Eurasia	Tropical forest	−0.0833*	NS
	Temperate broadleaf forests	0.1362***	0.517***
	Temperate conifer forests	0.1295***	0.6211***
	Tropical and subtropical grasslands, savannas and shrublands	NS	NS
	Temperate and montane grasslands, savannas and shrublands	0.0875**	0.3798**
	Boreal forests/taiga and tundra	NS	NS
	Mediterranean forests, woodlands and scrub	0.2877***	0.7607***
	Xeric shrublands	0.1435**	0.4243***
Australia/New Zealand	Tropical forest	NS	NS
	Temperate broadleaf forests	NS	NS
	Tropical and subtropical grasslands, savannas and shrublands	NS	NS
	Temperate and montane grasslands, savannas and shrublands	NS	NS
	Mediterranean forests, woodlands and scrub	NS	NS
	Xeric shrublands	NS	NS
North America	Tropical forest	0.3297***	0.454**
	Temperate broadleaf forests	NS	NS
	Temperate conifer forests	0.184***	0.4215**
	Tropical and subtropical grasslands, savannas and shrublands	NS	NS
	Temperate and montane grasslands, savannas and shrublands	NS	NS
	Boreal forests/taiga and tundra	NS	NS
	Mediterranean forests, woodlands and scrub	NS	NS
	Xeric shrublands	0.4156***	0.6618**
South America	Tropical forest	0.1461**	NS
	Temperate broadleaf forests	−0.1143***	NS
	Tropical and subtropical grasslands, savannas and shrublands	0.5027***	0.9297***
	Temperate and montane grasslands, savannas and shrublands	−1.4452***	−1.1156,***
	Xeric shrublands	0.4307*	0.6813**

NS, not significant.
Results of non-parametric tests examining temporal trends in the continental-level, biome mean fire weather season length and long fire weather season affected area. Shaded areas indicate either an absence or a very low percentage cover of that biome on that continent. All area trends are expressed as the percentage change of the total area of each biome on each continent (***$P<0.01$, **$P<0.05$, *$P<0.1$). Slopes were estimated using the Theil–Sen non-parametric trend slope estimator and significance tests were performed using the Mann–Kendall trend test following a four-step approach to reduce the effects of serial autocorrelation on trend test[66].

positive feedback to global atmospheric carbon accumulations if all the requirements for wildfires are present. In addition, this study may improve our ability to explore the complex drivers of global fire activity by isolating the climate-induced variations in fire potential from changes in either fuel availability or human and nature-caused ignitions, which lead to the realized burned

Table 4 | Correlations between fire weather season length metrics and reported nationwide burned area.

Country	Time period	Fire weather season length	Long fire weather season affected area
Canada[68]	1979–2013	0.30* (34)	0.324*NS (34)
United States[44]	1979–2013	0.679*** (21)	0.663*** (21)
United States[44]	1992–2013	0.683*** (34)	0.715*** (34)
Spain[69]	1980–2013	0.703*** (33)	0.743*** (27)
Portugal[69]	1980–2013	0.659*** (33)	0.67*** (19)
Italy[69]	1980–2013	0.823*** (33)	0.772*** (27)
France[69]	1980–2013	0.469*** (33)	NS
Greece[69]	1980–2013	0.611*** (33)	NS
Latvia[69]	1980–2013	0.694*** (33)	0.845** (10)

NS, not significant.
Spearman's rank-order correlation between detrended fire weather season length, long fire weather season affected area and log-transformed national burned area data reported for two countries in North America and six countries in Europe (***$P<0.01$, **$P<0.05$, *$P<0.1$). Canadian burned area was limited to boreal forests where most of the burned area occurs[70]. Number of data points after detrending are reported in parentheses.

Table 5 | Correlations between fire weather season length metrics and global net land carbon flux by continent and biome.

Continent	Biome	Correlation between mean fire weather season length and global net land carbon flux	Correlation between long fire weather season affected area and global net land carbon flux
Africa	Tropical forest	NS	NS
	Tropical and subtropical grasslands, savannas and shrublands	−0.358**	−0.431**
	Temperate and montane grasslands, savannas and shrublands	NS	NS
	Mediterranean forests, woodlands and scrub	NS	NS
	Xeric shrublands	NS	NS
Eurasia	Tropical forest	NS	NS
	Temperate broadleaf forests	NS	NS
	Temperate conifer forests	NS	−0.036
	Tropical and subtropical grasslands, savannas and shrublands	NS	NS
	Temperate and montane grasslands, savannas and shrublands	NS	NS
	Boreal forests/taiga and tundra	NS	NS
	Mediterranean forests, woodlands and scrub	NS	−0.377**
	Xeric shrublands	0.381**	0.467***
Australia/New Zealand	Tropical forest	−0.292*	NS
	Temperate broadleaf forests	NS	NS
	Tropical and subtropical grasslands, savannas and shrublands	NS	NS
	Temperate and montane grasslands, savannas and shrublands	NS	NS
	Mediterranean forests, woodlands and scrub	NS	−0.325*
	Xeric shrublands	NS	NS
North America	Tropical forest	NS	−0.299*
	Temperate broadleaf forests	NS	NS
	Temperate conifer forests	NS	NS
	Tropical and subtropical grasslands, savannas and shrublands	NS	0.341*
	Temperate and montane grasslands, savannas and shrublands	NS	NS
	Boreal forests/taiga and tundra	NS	NS
	Mediterranean forests, woodlands and scrub	NS	NS
	Xeric shrublands	NS	NS
South America	Tropical forest	−0.414**	−0.489***
	Temperate broadleaf forests	NS	−0.434**
	Tropical and subtropical grasslands, savannas and shrublands	−0.456***	−0.396**
	Temperate and montane grasslands, savannas and shrublands	NS	NS
	Xeric shrublands	−0.545***	−0.397**

NS, not significant.
Spearman's rank-order correlation coefficients between first-difference detrended global net land carbon flux and continental-level, biome mean fire weather season length and long fire weather season affected area (***$P<0.01$, **$P<0.05$, *$P<0.1$).

area and subsequent fire emissions. In summary, we have shown that combined surface weather changes over the last three and a half decades have promoted global wildfire weather season lengthening. If these trends continue, increased wildfire potential may have pronounced global socio-economic, ecological and climate system impacts.

Table 6 | Distribution of significant trends in fire weather season length and long fire weather season affected area by continent and biome.

Continent	Biome	Min	1st quarter	Median	3rd quarter	Max	N
Africa	Tropical forest	−1.33	−0.116	0.287	0.641	2.120	147
	Tropical and subtropical grasslands, savannas and shrublands	−1.790	0.668	0.597	1.11	2.22	853
	Temperate and montane grasslands, savannas and shrublands	−0.75	−0.333	0.254	0.448	1.76	30
	Mediterranean forests, woodlands and scrub	0.205	0.306	0.360	0.465	0.775	29
	Xeric shrublands	−1.55	−0.867	0.477	1.10	1.98	141
Eurasia	Tropical forest	−1.04	−0.295	0.0417	0.114	1.46	335
	Temperate broadleaf forests	0.257	0.106	0.161	0.271	2.02	642
	Temperate conifer forests	−0.318	0.0767	0.114	0.248	2.14	158
	Tropical and subtropical grasslands, savannas and shrublands	−0.578	0.059	0.0715	0.111	0.179	5
	Temperate and montane grasslands, savannas and shrublands	−1.14	0.0608	0.182	0.2590	1.62	659
	Boreal forests/taiga and tundra	−0.496	−0.136	−0.0519	0.063	0.251	711
	Mediterranean forests, woodlands and scrub	−0.285	0.336	0.414	0.542	0.83	123
	Xeric shrublands	−1.22	−0.252	0.363	0.665	2.15	563
Australia/New Zealand	Tropical forest	−0.537	−0.523	−0.429	−0.172	1.67	4
	Temperate broadleaf forests	0.0932	0.108	0.147	0.153	0.301	25
	Tropical and subtropical grasslands, savannas and shrublands	−1.34	−0.965	−0.633	0.49	0.968	51
	Temperate and montane grasslands, savannas and shrublands	0.0428	0.106	0.111	0.13	0.13	35
	Mediterranean forests, woodlands and scrub	−0.559	−0.278	0.181	0.315	0.341	9
	Xeric shrublands	−1.09	−0.703	−0.548	−0.291	0.439	62
North America	Tropical forest	−0.364	0.391	0.719	1.28	1.97	112
	Temperate broadleaf forests	−0.264	0.0492	0.105	0.17	0.228	66
	Temperate conifer forests	−0.222	0.0315	0.246	0.441	1.03	288
	Tropical and subtropical grasslands, savannas and shrublands	0.119	0.126	0.133	0.141	0.148	2
	Temperate and montane grasslands, savannas and shrublands	0.0469	0.261	0.322	0.464	0.813	120
	Boreal forests/taiga and tundra	−0.302	−0.10	0.0399	0.0731	0.264	809
	Mediterranean forests, woodlands and scrub	−0.823	0.624	0.761	0.893	1.410	16
	Xeric shrublands	0.162	0.433	0.56	0.681	1.210	287
South America	Tropical forest	−1.76	−0.0863	0.252	0.731	2.04	706
	Temperate broadleaf forests	−2.53	−0.557	0.0288	0.0957	0.275	36
	Tropical and subtropical grasslands, savannas and shrublands	−0.887	0.62	0.947	1.30	2.39	320
	Temperate and montane grasslands, savannas and shrublands	−2.64	−0.829	−0.375	0.302	0.966	258
	Xeric shrublands	−2.660	−0.588	1.440	1.650	2.070	112

Statistical summaries of all significant, pixel-based fire weather season length linear trends from 1979 to 2013 by biome for Africa and Eurasia. All values are trend coefficients in days per year, representing an increase or decrease in the fire weather season length. *N* represents the number of significant pixels in each continent × biome. Slopes were estimated using the Theil–Sen non-parametric trend slope estimator.

Methods

Meteorological data. Three global reanalysis projects provided gridded, sub-daily surface meteorological data from 1979 to 2013. Two data sets at ~210 km spatial resolution were obtained from NCEP, including the Reanalysis I[36] and the DOE Reanalysis II data sets[37]. Six-hourly data fields for 2 m maximum temperature, minimum temperature, specific humidity, surface pressure, precipitation rate, water equivalent of actual snow depth and 10 m *U* and *V* wind components were summarized to daily data (Supplementary Table 2). We assumed that diurnal variations in actual vapour pressure are small and thus daily mean actual vapour pressure was calculated from the NCEP data using mean daily specific humidity and surface pressure[65], and saturation vapour pressure was calculated from daily maximum and minimum temperature to calculate daily maximum and minimum relative humidity. In addition, we used the ECMWF ERA Interim Reanalysis[35]. This data set is similar to NCEP's but at a higher spatial and temporal resolution (~78 km resolution). We extracted 3-hourly 2 m air temperature, dewpoint temperature, surface total precipitation, and 10 m *U* and *V* wind components using the ECMWF GRIdded Binary Application Programming Interface (GRIB-API) and used them to derive daily maximum and minimum temperature, maximum and minimum relative humidity, maximum wind and total daily precipitation amount and daily precipitation duration (Supplementary Table 3). Daily maximum and minimum relative humidity were calculated using mean daily dewpoint temperature and minimum and maximum daily 2 m air temperature, respectively.

Surface meteorological data analysis. Trends in ensemble mean annual values were analysed for five climate variables that are important to wildland fire potential: mean maximum daily temperature, mean minimum daily relative humidity, total precipitation, rain-free days and mean maximum 10 m wind speed. Annual means or totals for each pixel were averaged across all three reanalysis data sets to produce an ensemble mean value. Two types of analysis were performed on each ensemble climate variable. First, we examined areas that showed long-term trends in mean annual weather conditions. All trends were evaluated using Mann–Kendall trend tests, following a four-step process to reduce the effects of serial autocorrelation on significance tests[66] (see Supplemental Methods). Second, we examined the change in frequency of occurrence of unusually hot, dry or windy conditions by comparing the number of years that maximum temperature, rain-free days or wind speed was >1 s.d. above the mean or when minimum relative humidity was <1 s.d. from the mean in 1996–2013, as compared with the number of similar events observed in 1979–1996. One year, 1996, overlaps each period to provide 18 years in each period. Further, all data sets were masked using the vegetated (burnable) land area defined by a global landcover data set developed from AVHRR satellite data[67]. Mean trends and event frequency changes were then displayed spatially (Fig. 1) and summarized to average global values (Supplementary Table 1).

References

1. Bowman D. M. J. S. *et al.* Fire in the Earth system. *Science* **324,** 481–484 (2009).
2. Giglio, L., Randerson, J. T. & van der Werf, G. R. Analysis of daily, monthly, and annual burned area using the fourth generation global fire emissions database (GFED4). *J. Geophys. Res.* **118,** 317–328 (2013).
3. Andreae, M. O. & Merlet, P. Emission of trace gases and aerosols from biomass burning. *Glob. Biogeochem. Cycles* **15,** 955–966 (2001).
4. Intergovernmental Panel on Climate Change (IPCC). Climate change 2007: *The Physical Science Basis.* (Cambridge Univ. Press, 2007).
5. van der Werf, G. R. *et al.* Interannual variability in global biomass burning emissions from 1997 to 2004. *Atmos. Chem. Phys.* **6,** 3423–3441 (2006).
6. Bowman D. M. J. S. *et al.* The human dimension of fire regimes on Earth. *J. Biogeogr.* **38,** 2223–2236 (2011).

7. National Interagency Fire Center. *Federal firefighting costs (suppression only)* https://www.nifc.gov/fireInfo/fireInfo_documents/SuppCosts.pdf, 2013).
8. González-Cabán, A. *Vegetation Fires and Global Change: Challenges for Concerted International Action* (Global Fire Monitoring Center (GFMC), 2013).
9. Ashe, B. S. W., McAneny, K. J. & Pitman, A. J. in *Proceedings of the Third International Symposium on Fire Economics, Planning and Policy: Common Problems and Approaches*. 29 April, 2 May 2008. (US Department of Agriculture, Forest Service Pacific Southwest Research Station, Albany, CA, USA, 2009).
10. Moritz, M. A., Morais, M. E., Summerell, L. A., Carlson, J. M. & Doyle, J. Wildfires, complexity, and highly optimized tolerance. *Proc. Natl Acad. Sci. USA* **102,** 17912–17917 (2005).
11. Abatzoglou, J. T. & Kolden, C. A. Relationships between climate and macroscale area burned in the western United States. *Int. J. Wildland Fire* **22,** 1003–1020 (2013).
12. Bessie, W. C. & Johnson, E. A. The relative importance of fuels and weather on fire behaviour in subalpine forests. *Ecology* **76,** 747–762 (1995).
13. Flannigan, M. D., Logan, K. A., Amiro, B. D., Skinner, W. R. & Stocks, B. J. Future area burned in Canada. *Clim. Change* **72,** 1–16 (2005).
14. Littell, J. S., McKenzie, D., Peterson, D. L. & Westerling, A. L. Climate and wildfire area burned in western US ecoprovinces, 1916-2003. *Ecol. Appl.* **19,** 1003–1021 (2009).
15. Flannigan, M. D. & Harrington, J. B. A study of the relation of meteorological variables to monthly provincial area burned by wildfire in Canada (1953-80). *J. Appl. Meteorol.* **27,** 441–452 (1988).
16. Hansen, J., Ruedy, R., Sato, M. & Lo, K. Global surface temperature change. *Rev. Geophys.* **48,** RG4004 (2010).
17. Trenberth, K. E., Dai, A., Rasmussen, R. M. & Parsons, D. B. The changing character of precipitation. *Bull. Am. Meteorol. Soc.* **84,** 1205–1217 (2003).
18. Dai, A. Increasing drought under global warming in observations and models. *Nat. Clim. Change* **3,** 52–58 (2013).
19. Sheffield, J., Wood, E. F. & Roderick, M. L. Little change in global drought over the past 60 years. *Nature* **491,** 435–438 (2012).
20. Dessler, A. E., Zhang, Z. & Yang, P. Water-vapour climate feedback inferred from climate fluctuations, 2003–2008. *Geophys. Res. Lett.* **35,** L20704 (2008).
21. Shabbar, A. & Skinner, W. Summer drought patterns in Canada and the relationship to global sea surface temperatures. *J. Clim.* **17,** 2866–2880 (2004).
22. Girardin, M. P. & Wotton, B. M. Summer moisture and wildfire risks across Canada. *J. Appl. Meteorol. Climatol.* **48,** 517–533 (2009).
23. Flannigan, M. D., Krawchuk, M. A., de Groot, W. J., Wotton, B. M. & Gowman, L. M. Implications of changing climate for global wildland fire. *Int. J. Wildland Fire* **18,** 483–507 (2009).
24. Flannigan, M. *et al.* Global wildland fire season severity in the 21st century. *For. Ecol. Manag.* **294,** 54–61 (2013).
25. Clarke, H., Lucas, C. & Smith, P. Changes in Australian fire weather between 1973 and 2010. *Int. J. Climatol.* **33,** 931–944 (2013).
26. Girardin, M. P. *et al.* Heterogeneous response of circumboreal wildfire risk to climate change since the early 1900s. *Glob. Change Biol.* **15,** 2751–2769 (2009).
27. Groisman, P. Y. *et al.* Potential forest fire danger over Northern Eurasia: changes during the 20th century. *Glob. Planet. Change* **56,** 371–386 (2007).
28. Tian, X.-r., Zhao, F.-j., Shu, L.-f. & Wang, M.-y. Changes in forest fire danger for south-western China in the 21st century. *Int. J. Wildland Fire* **23,** 185–195 (2014).
29. Venäläinen, A. *et al.* Temporal variations and change in forest fire danger in Europe for 1960–2012. *Nat. Hazards Earth Syst. Sci.* **14,** 1477–1490 (2014).
30. Albert-Green, A., Dean, C., Martell, D. L. & Woolford, D. G. A methodology for investigating trends in changes in the timing of the fire season with applications to lightning-caused forest fires in Alberta and Ontario, Canada. *Can. J. For. Res.* **43,** 39–45 (2012).
31. Wotton, B. M. Interpreting and using outputs from the Canadian Forest Fire Danger Rating System in research applications. *Environ. Ecol. Stat.* **16,** 107–131 (2009).
32. Andrews, P. L., Loftsgaarden, D. O. & Bradshaw, L. S. Evaluation of fire danger rating indexes using logistic regression and percentile analysis. *Int. J. Wildland Fire* **12,** 213–226 (2003).
33. Carvalho, A., Flannigan, M. D., Logan, K., Miranda, A. I. & Borrego, C. Fire activity in Portugal and its relationship to weather and the Canadian Fire Weather Index System. *Int. J. Wildland Fire* **17,** 328–338 (2008).
34. Brown, J. K., Reinhardt, E. D. & Fischer, W. C. Predicting Duff and Woody fuel consumption in Northern Idaho prescribed fires. *For. Sci.* **37,** 1550–1566 (1991).
35. Dee, D. P. *et al.* The ERA-Interim reanalysis: configuration and performance of the data assimilation system. *Q. J. R. Meteorol. Soc.* **137,** 553–597 (2011).
36. Kalnay, E. *et al.* The NCEP/NCAR 40-year reanalysis project. *Bull. Am. Meteorol. Soc.* **77,** 437–471 (1996).
37. Kanamitsu, M. *et al.* NCEP-DOE AMIP-II Reanalysis (R-2). *Bull. Am. Meteorol. Soc.* **83,** 1631–1643 (2002).
38. Bradshaw, L. S., Deeming, J. E., Burgan, R. E. & Cohen, J. D. The 1978 NFDRS: technical documentation. USDA Forest Service, Report No. Gen Tech Rep INT-169, 44 (U.S. Department of Agriculture, Forest Service, Intermountain Forest and Range Experiment Station, Missoula, MT, USA, 1983).
39. Van Wagner, C. E. Development and structure of the Canadian forest fire weather index system. Report No. 1992 (Canadian Forestry Service, Petawawa National Forestry Institute, Chalk River, ON, Canada, 1987).
40. Noble, I. R., Gill, A. M. & Bary, G. A. V. McArthur's fire-danger meters expressed as equations. *Aust. J. Ecol.* **5,** 201–203 (1980).
41. de Beurs, K. M. & Henebry, G. M. *Phenological Research* (Springer, 2010).
42. White, M. A., Thornton, P. E. & Running, S. W. A continental phenology model for monitoring vegetation responses to interannual climatic variability. *Glob. Biogeochem. Cycles* **11,** 217–234 (1997).
43. Hagedorn, R., Doblas-Reyes, F. J. & Palmer, T. N. The rationale behind the success of multi-model ensembles in seasonal forecasting--I. Basic concept. *Tellus A* **57,** 219–233 (2005).
44. National Interagency Fire Center. Total Wildland Fires and Acres (1960-2013) <http://www.nifc.gov/fireInfo/fireInfo_stats_totalFires.html> (2014).
45. Short, K. A spatial database of wildfires in the United States, 1992-2011. *Earth Syst. Sci. Data* **6,** 1–27 (2014).
46. Page, S. E. *et al.* The amount of carbon released from peat and forest fires in Indonesia during 1997. *Nature* **420,** 61–65 (2002).
47. Girardin, M. P. Interannual to decadal changes in area burned in Canada from 1781 to 1982 and the relationship to Northern Hemisphere land temperatures. *Glob. Ecol. Biogeogr.* **16,** 557–566 (2007).
48. Le Quéré, C. *et al.* Global carbon budget 2013. *Earth Syst. Sci. Data* **6,** 235–263 (2014).
49. Spanish Ministry of Agriculture FaE. Incendios Forestales en España 1 enero—31 diciembre 2012. (Government of Spain, Ministry of Agriculture, Food and Environment, Madrid, Spain (ES), http://www.fire.uni-freiburg.de/inventory/stat/es/Advance-Wildland-Fire-Report-Spain-2012.pdf (2012).
50. Nicholson, S. E. The nature of rainfall fluctuations in subtropical West Africa. *Mon. Weather Rev.* **108,** 473–487 (1980).
51. Zvyagintsev, A. M. *et al.* Air pollution over European Russia and Ukraine under the hot summer conditions of 2010. *Izv. Atmos. Ocean Phys.* **47,** 699–707 (2011).
52. Terrier, A., de Groot, W. J., Girardin, M. P. & Bergeron, Y. Dynamics of moisture content in spruce–feather moss and spruce–Sphagnum organic layers during an extreme fire season and implications for future depths of burn in Clay Belt black spruce forests. *Int. J. Wildland Fire* **23,** 490–502 (2014).
53. Dennison, P. E., Brewer, S. C., Arnold, J. D. & Moritz, M. A. Large wildfire trends in the western United States, 1984–2011. *Geophys. Res. Lett.* **41,** 2928–2933 (2014).
54. Westerling, A. L., Hidalgo, H. G., Cayan, D. R. & Swetnam, T. W. Warming and earlier spring increase Western U.S. forest wildfire activity. *Science* **313,** 940–943 (2006).
55. Williams, A. P. *et al.* Temperature as a potent driver of regional forest drought stress and tree mortality. *Nat. Clim. Change* **3,** 292–297 (2013).
56. Holden, Z. A., Morgan, P., Crimmins, M. A., Steinhorst, R. K. & Smith, A. M. S. Fire season precipitation variability influences fire extent and severity in a large southwestern wilderness area, United States. *Geophys. Res. Lett.* **34,** L16708 (2007).
57. Timmons, R. S., deBano, L. & Ryan, K. C. Implications of Fire Management on Cultural Resources. Report No. RMRS-GTR-42 vol. 3 (Fort Collins, CO., 2012).
58. Zeng, N. *et al.* Causes and impacts of the 2005 Amazon drought. *Environ. Res. Lett.* **3,** 014002 (2008).
59. Cochrane, M. A. & Barber, C. P. Climate change, human land use and future fires in the Amazon. *Glob. Change Biol.* **15,** 601–612 (2009).
60. Cochrane, M. A. Fire science for rainforests. *Nature* **421,** 913–919 (2003).
61. Cai, W. *et al.* Projected response of the Indian Ocean Dipole to greenhouse warming. *Nat. Geosci.* **6,** 999–1007 (2013).
62. Ropelewski, C. F. & Halpert, M. S. Global and regional scale precipitation patterns associated with the el niño/southern oscillation. *Mon. Weather Rev.* **115,** 1606–1626 (1987).
63. Nemani, R. R. *et al.* Climate-driven increases in global terrestrial net primary production from 1982 to 1999. *Science* **300,** 1560–1563 (2003).
64. Wang, W. *et al.* Variations in atmospheric CO_2 growth rates coupled with tropical temperature. *Proc. Natl Acad. Sci. USA* **110,** 13061–13066 (2013).
65. Bolton, D. The computation of equivalent potential temperature. *Mon. Weather Rev.* **108,** 1046–1053 (1980).
66. Yue, S., Pilon, P., Phinney, B. & Cavadias, G. The influence of autocorrelation on the ability to detect trend in hydrological series. *Hydrol. Process.* **16,** 1807–1829 (2002).
67. Hansen, M. R., DeFries, R. S., Townshend, J. R. G. & Sohlberg, R. Global land cover classification at 1km resolution using a decision tree classifier. *Int. J. Remote Sens.* **21,** 1331–1365 (2000).
68. Canadian National Forestry Database. Forest Fire Statistics by Province/Territory/Agency, 1970-2013 <http://nfdp.ccfm.org/data/compendium/html/comp_31e.html> (2014).

69. Schmuck, G. *et al.* Forest Fires in Europe, Middle East and North Africa 2013. Report No. EUR26791, (European Commission, Joint Research Centre, Institute for Environment and Sustainability, Ispra (VA), Italy, https://ec.europa.eu/jrc/sites/default/files/lb-na-26791-en-n.pdf (2014).
70. Stocks, B. *et al.* Large forest fires in Canada, 1959-1997. *J. Geophys. Res.* **108,** 1–12 (2003).

Acknowledgements

This work was supported by NASA Headquarters under the Terrestrial Ecology Program (NNX11AB89G) of the NASA Science Mission Directorate's Earth Science Division. Additional funding was provided by NASA through a NNH11ZDA001N-FIRES applied wildland fire sciences award. NCEP Reanalysis data was provided by the NOAA/OAR/ESRL PSD, Boulder, Colorado, USA, from their website at http://www.esrl.noaa.gov/psd/. NCEP-DOE AMIP-II Reanalysis (R-2) was produced with the support of the US National Weather Service and of PCMDI (US Dept. of Energy).

Author contributions

W.M.J. designed the study, collected data, performed all analyses and wrote the paper. M.A.C., P.H.F. and D.M.J.S.B. refined study design and analyses and co-wrote the paper. Z.A.H. refined analyses to include rain-free periods and co-wrote the paper. All other authors discussed results and co-wrote the paper.

Additional information

Supplementary Information accompanies this paper at http://www.nature.com/naturecommunications

Competing financial interests: The authors declare no competing financial interests.

Reprints and permission information is available online at http://npg.nature.com/reprintsandpermissions/

How to cite this article: Jolly, W. M. *et al.* Climate-induced variations in global wildfire danger from 1979 to 2013. *Nat. Commun.* 6:7537 doi: 10.1038/ncomms8537 (2015).

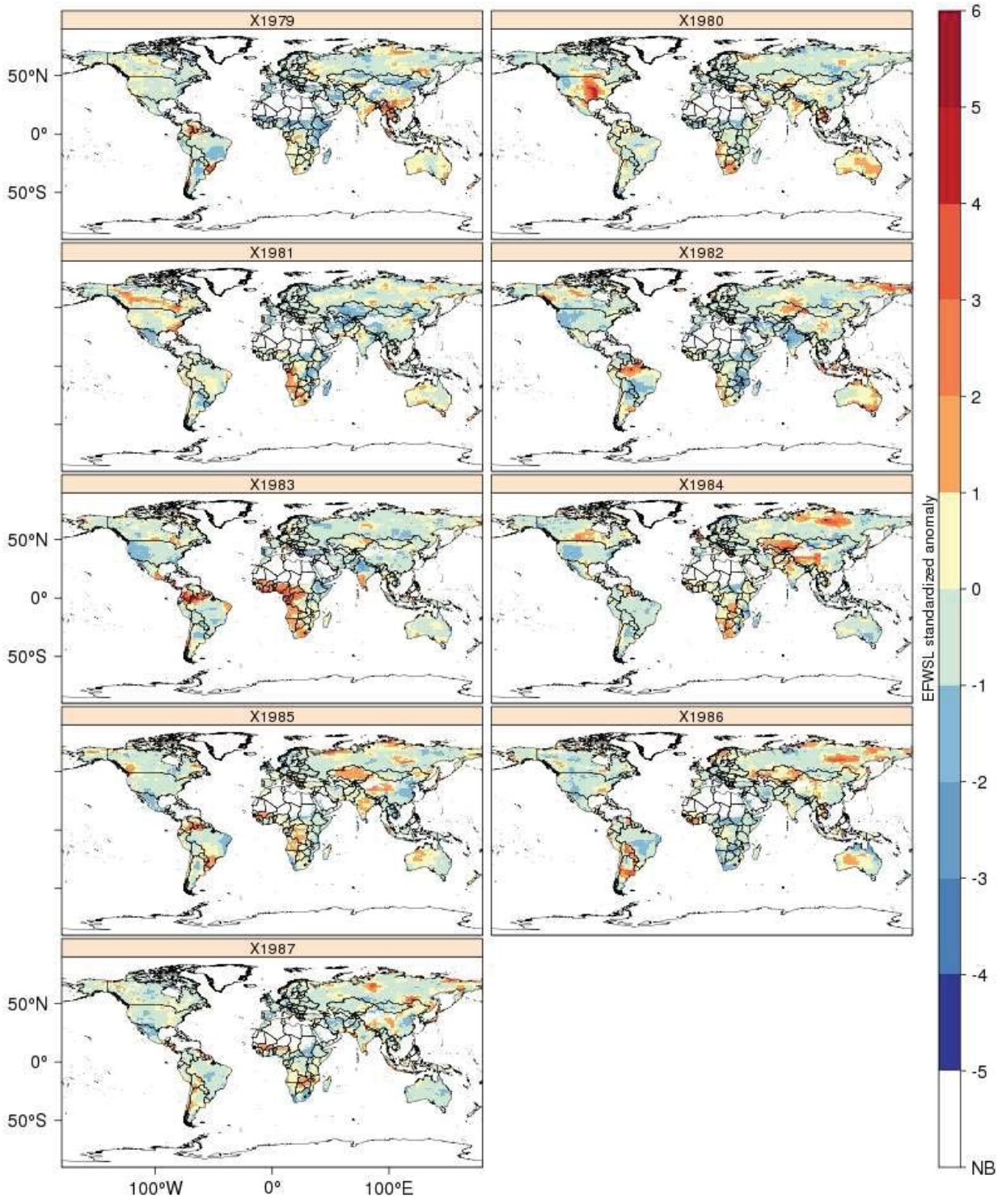

Supplementary Figure 1 – Maps of standardized anomalies of Fire Weather Season Length (Equation 5) from 1979-1987.

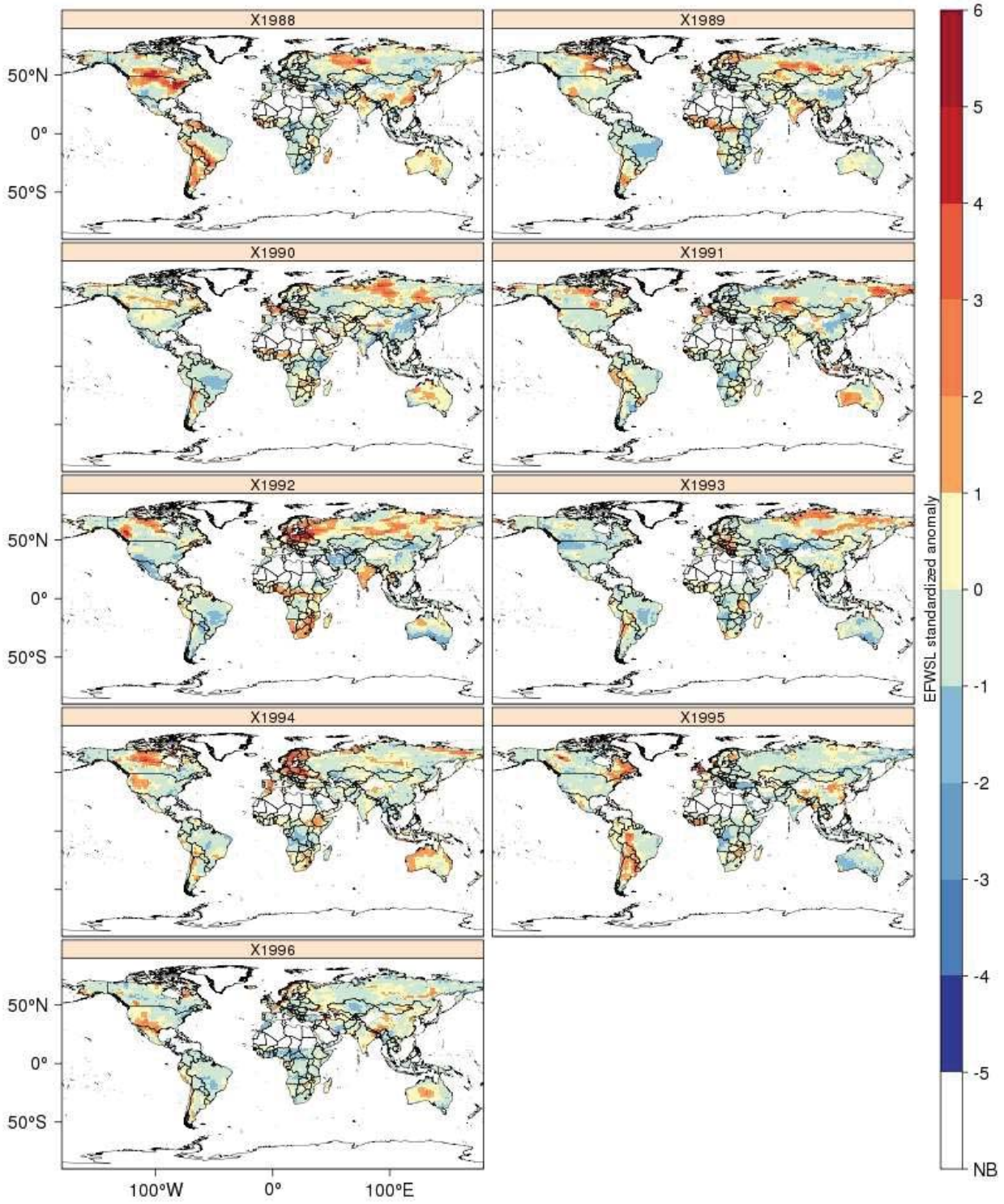

Supplementary Figure 2 – Maps of standardized anomalies of Fire Weather Season Length (Equation 5) from 1988-1996.

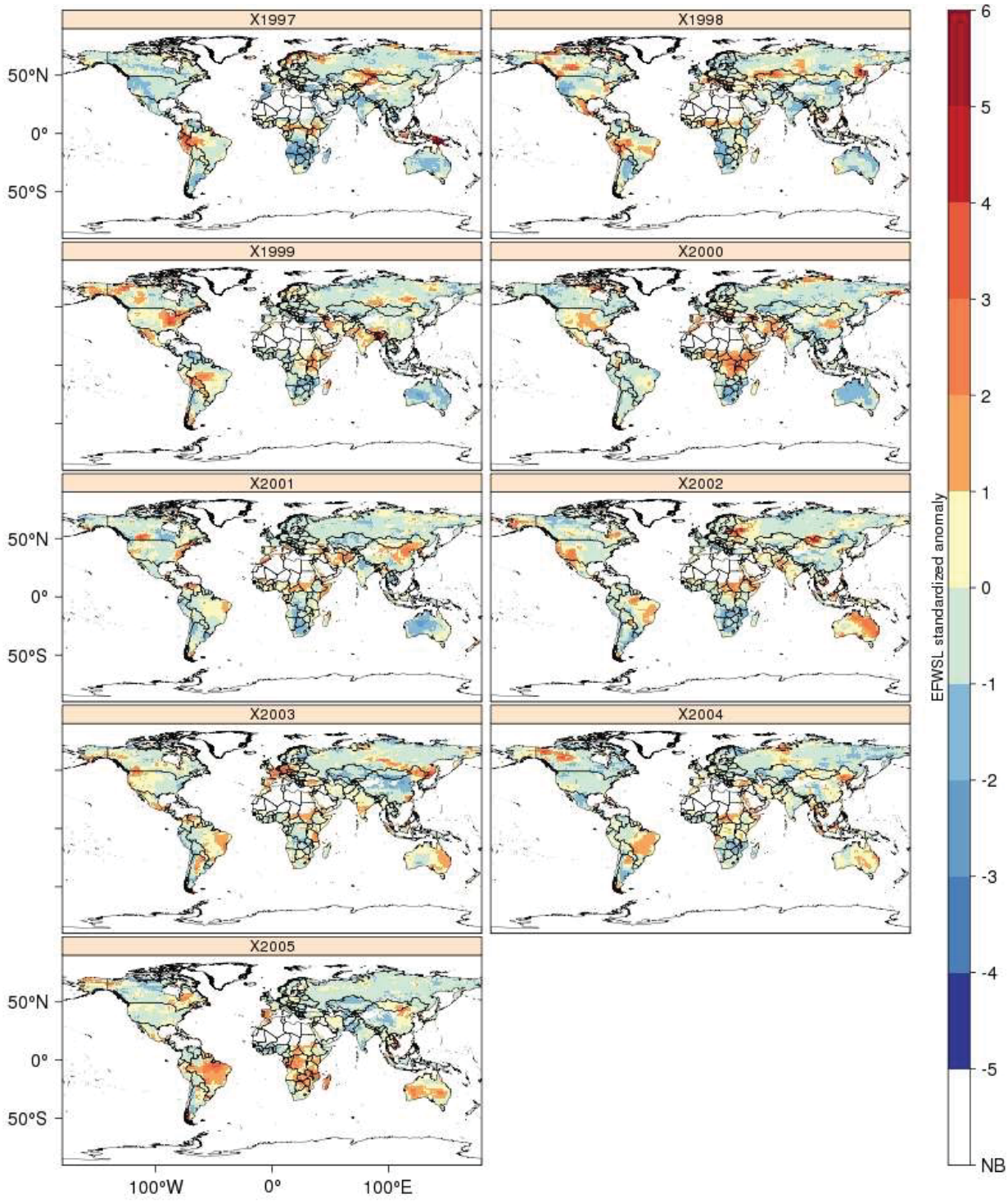

Supplementary Figure 3 – Maps of standardized anomalies of Fire Weather Season Length (Equation 5) from 1997-2005.

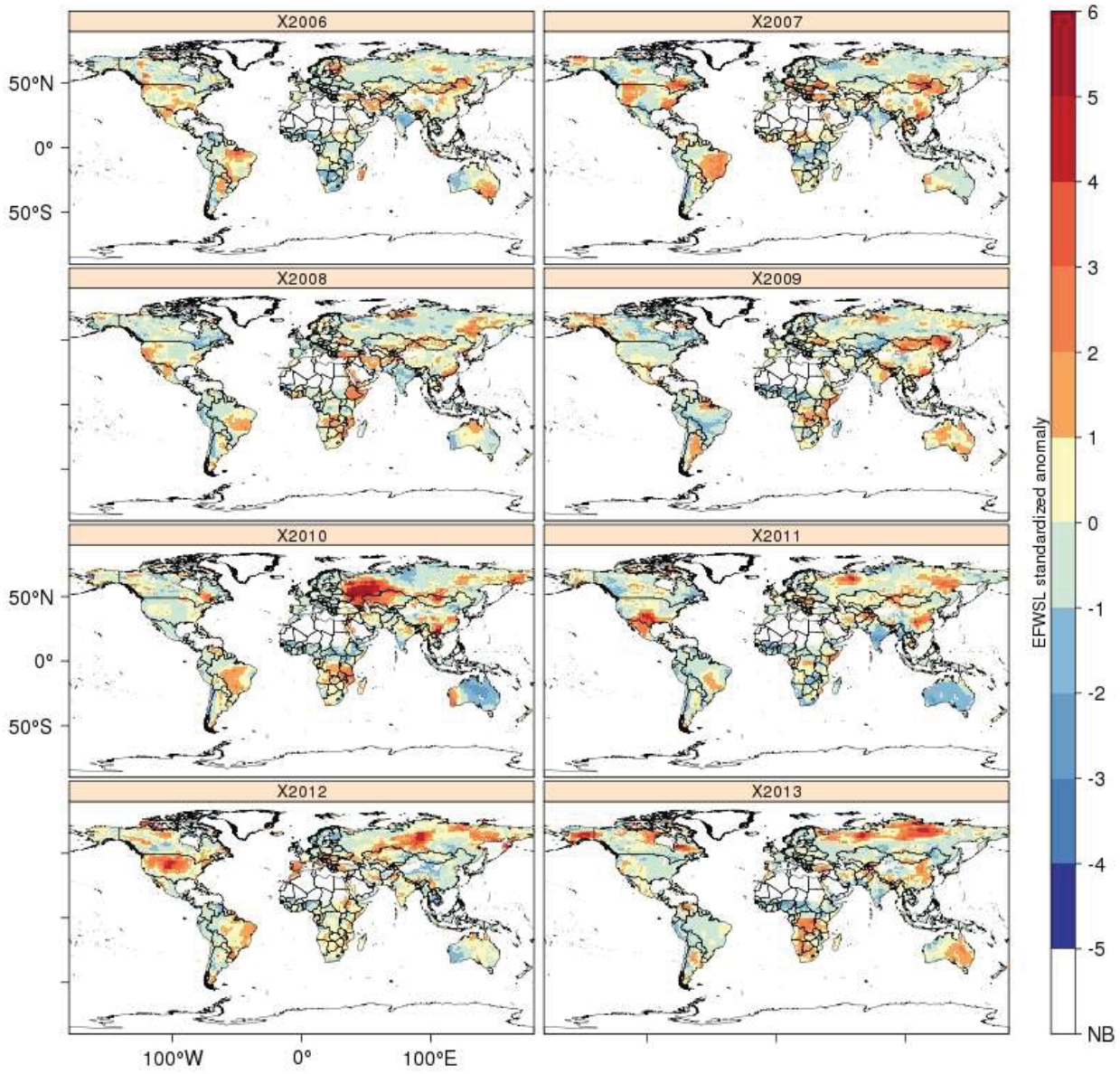

Supplementary Figure 4 – Maps of standardized anomalies of Fire Weather Season Length (Equation 5) from 2006-2013.

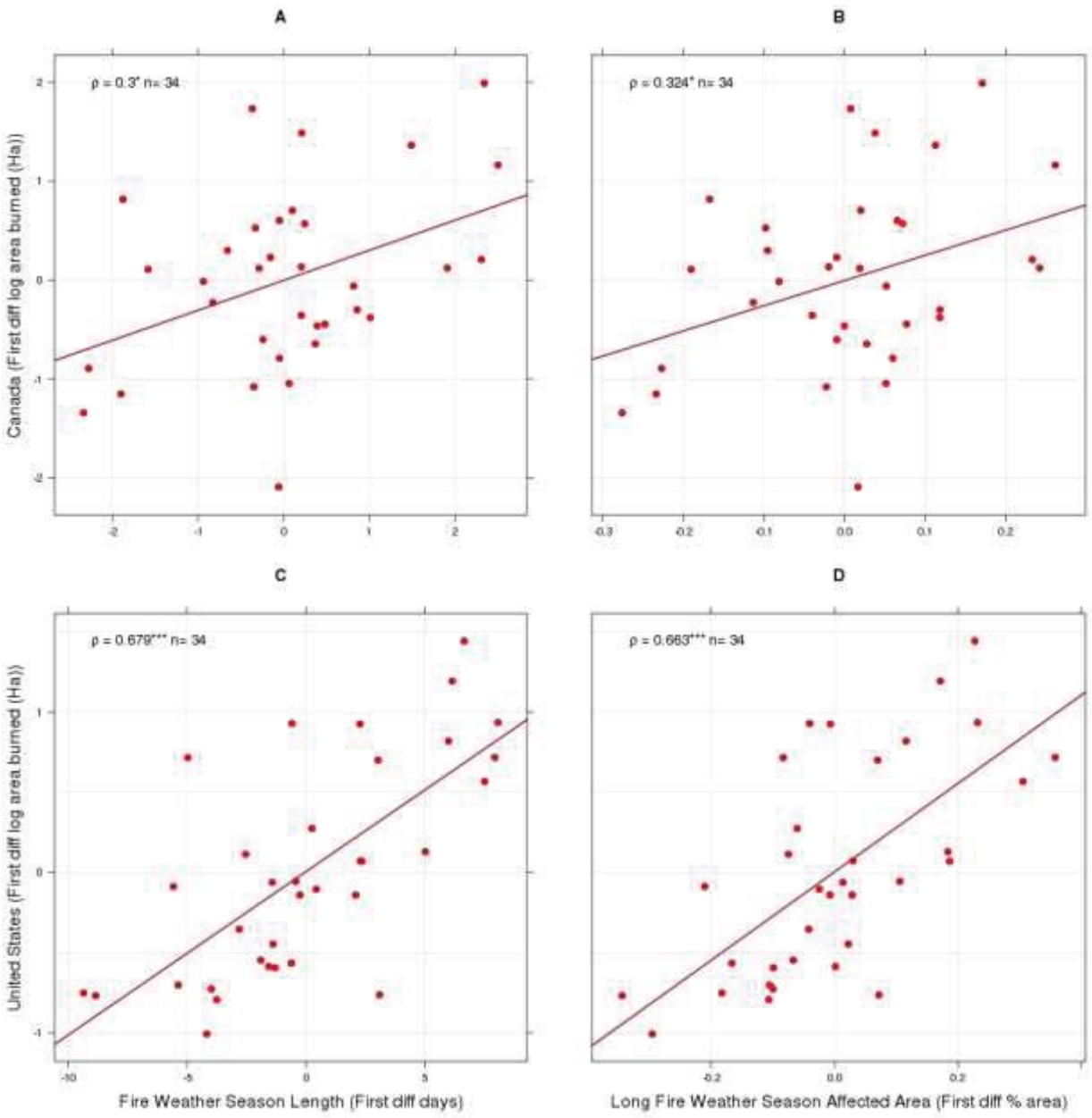

Supplementary Figure 5 – Comparisons of first-difference detrended spatial mean fire weather season length and long fire weather season affected area across Canada (A,B) and the United States (C,D) from 1979-2013. Neither fire weather season length nor long fire weather season affected was significantly related to burned area in Canadian forests but both season metrics were significantly related to burned area across the United States. Red lines show the estimated Theil-Sen trend slopes. Values reported in plot upper left are Spearman's rank-order correlation and corresponding significance (* p < 0.01, ** p < 0.05, * p < 0.1, NS Not Significant)**

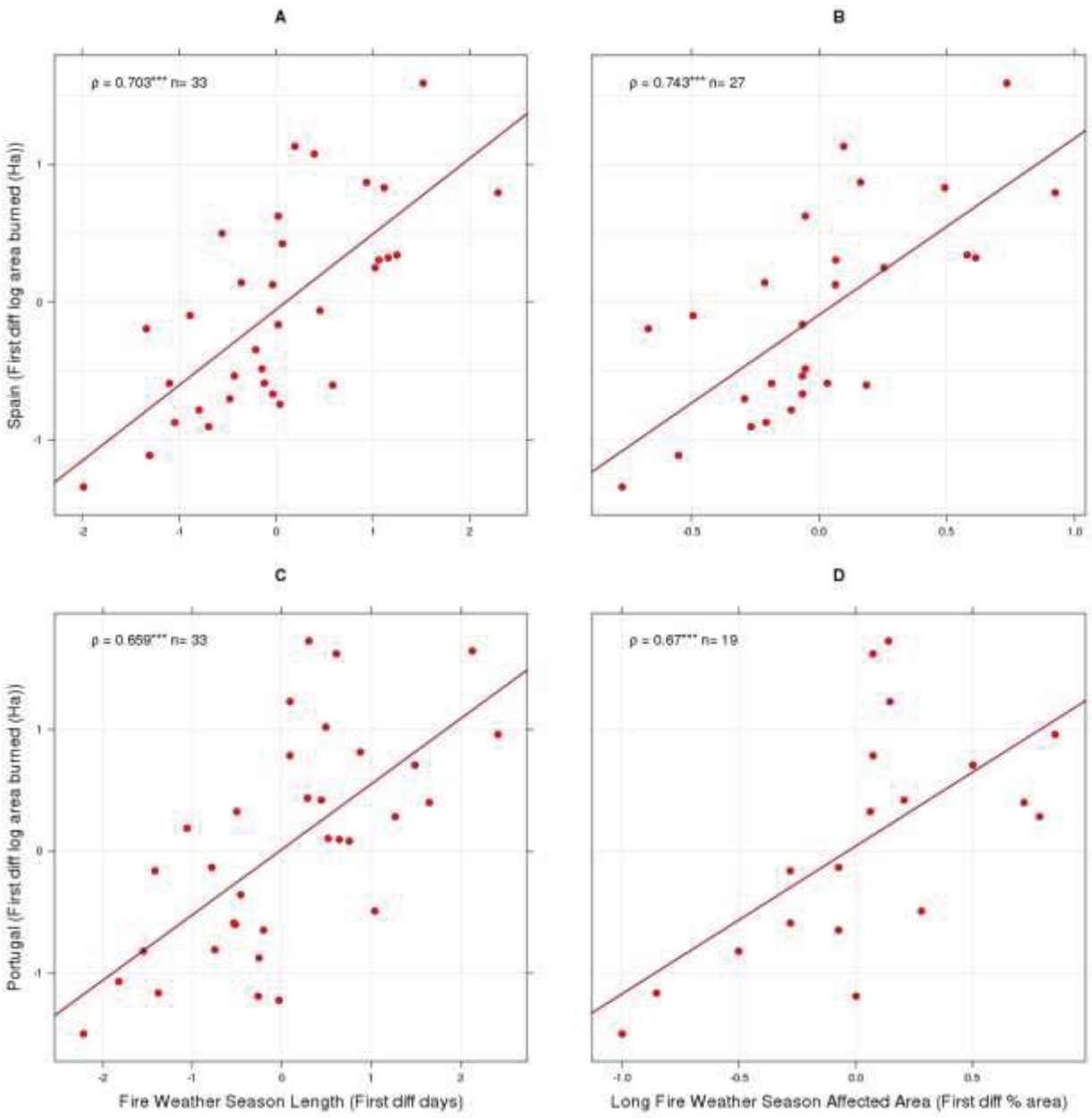

Supplementary Figure 6 – Comparisons of first-difference detrended spatial mean fire weather season length and long fire weather season affected area across Spain (A,B) and the Portugal (C,D) from 1980-2013. Both season metrics were significantly related to burned area across Spain and Portugal. Years where long fire weather season affected area was zero were excluded from analysis; therefore sample sizes for panels B and D are variable. Red lines show the estimated Theil-Sen trend slopes. Values reported in plot upper left are Spearman's rank-order correlation and corresponding significance (* p < 0.01, ** p < 0.05, * p < 0.1, NS Not Significant).**

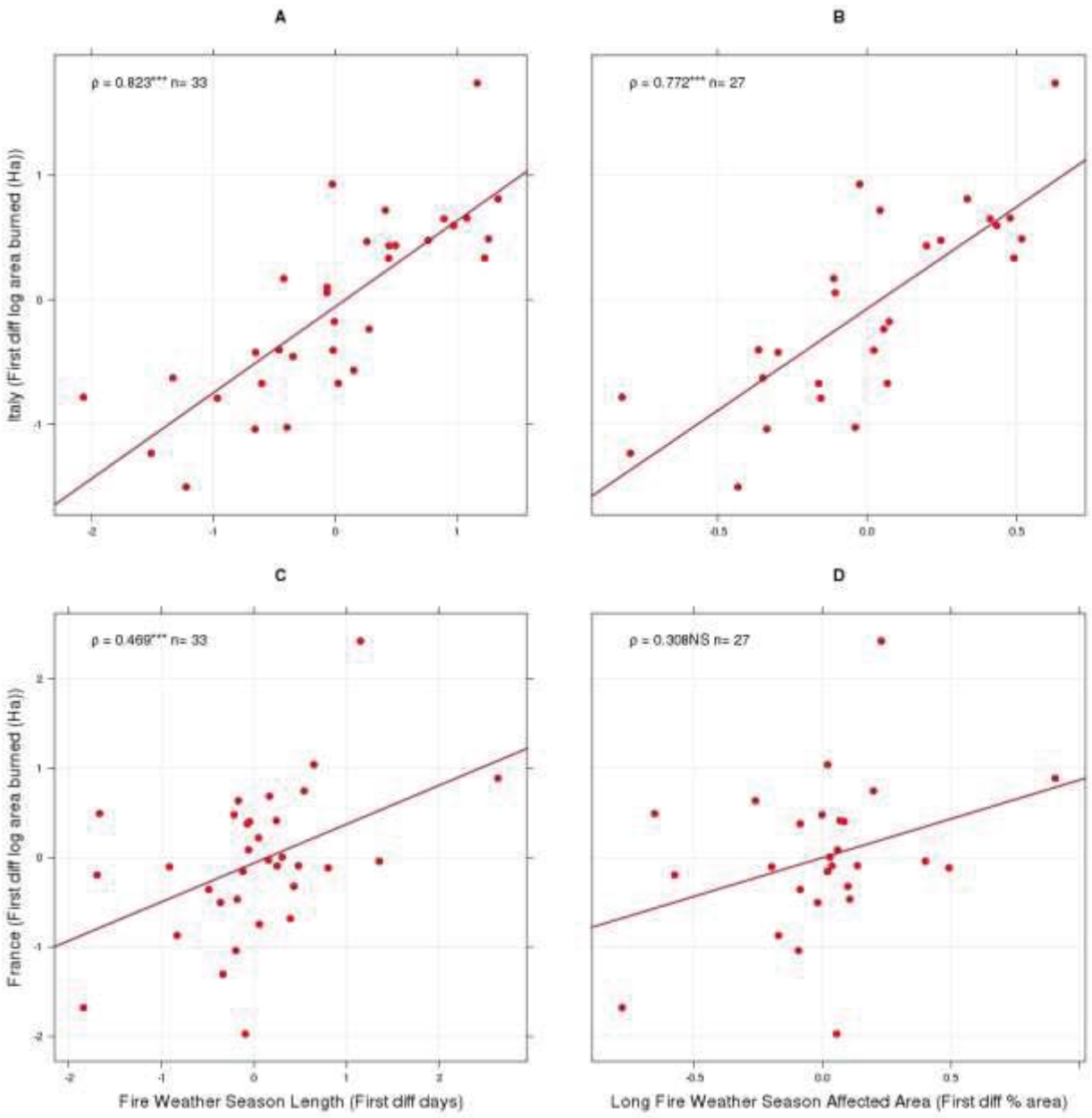

Supplementary Figure 7 – Comparisons of first-difference detrended spatial mean fire weather season length and long fire weather season affected area across Italy (A,B) and France (C,D) from 1980-2013. Fire weather season length was significantly related to burned area across both Italy and France and long fire weather season affected area was significantly correlated to burned area in Italy. Years where long fire weather season affected area was zero were excluded from analysis; therefore sample sizes for panels B and D are variable. Red lines show the estimated Theil-Sen trend slopes. Values reported in plot upper left are Spearman's rank-order correlation and corresponding significance (* p < 0.01, ** p < 0.05, * p < 0.1, NS Not Significant).**

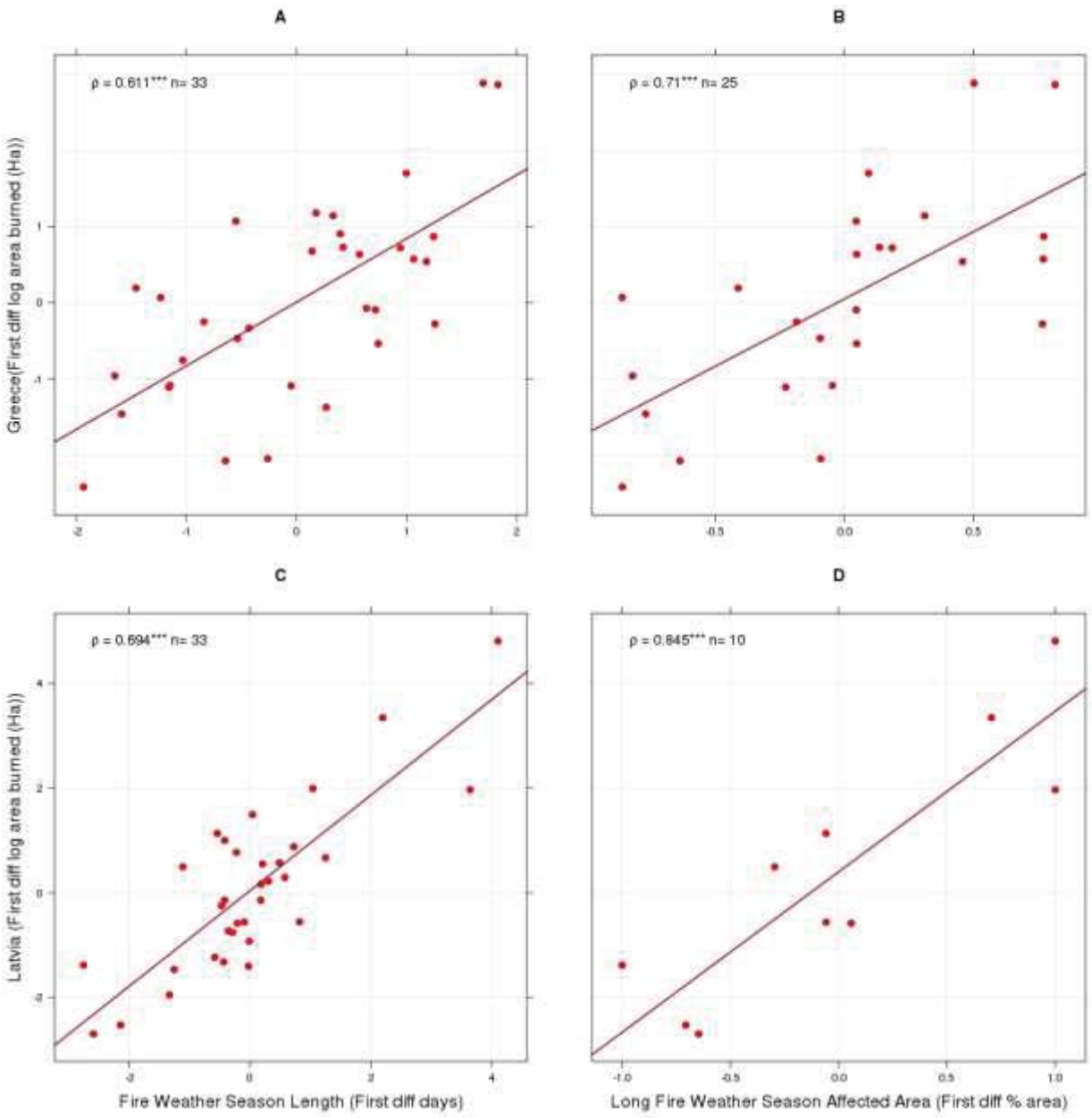

Supplementary Figure 8 – Comparisons of first-difference detrended spatial mean fire weather season length and long fire weather season affected area across Greece (A,B) and Latvia (C,D) from 1980-2013. Fire weather season length was significantly related to burned area across both Greece and Latvia and long fire weather season affected area was significantly correlated to burned area in Latvia. Years where long fire weather season affected area was zero were excluded from analysis; therefore sample sizes for panels B and D are variable. Red lines show the estimated Theil-Sen trend slopes. Values reported in plot upper left are Spearman's rank-order correlation and corresponding significance (* p < 0.01, ** p < 0.05, * p < 0.1, NS Not Significant).**

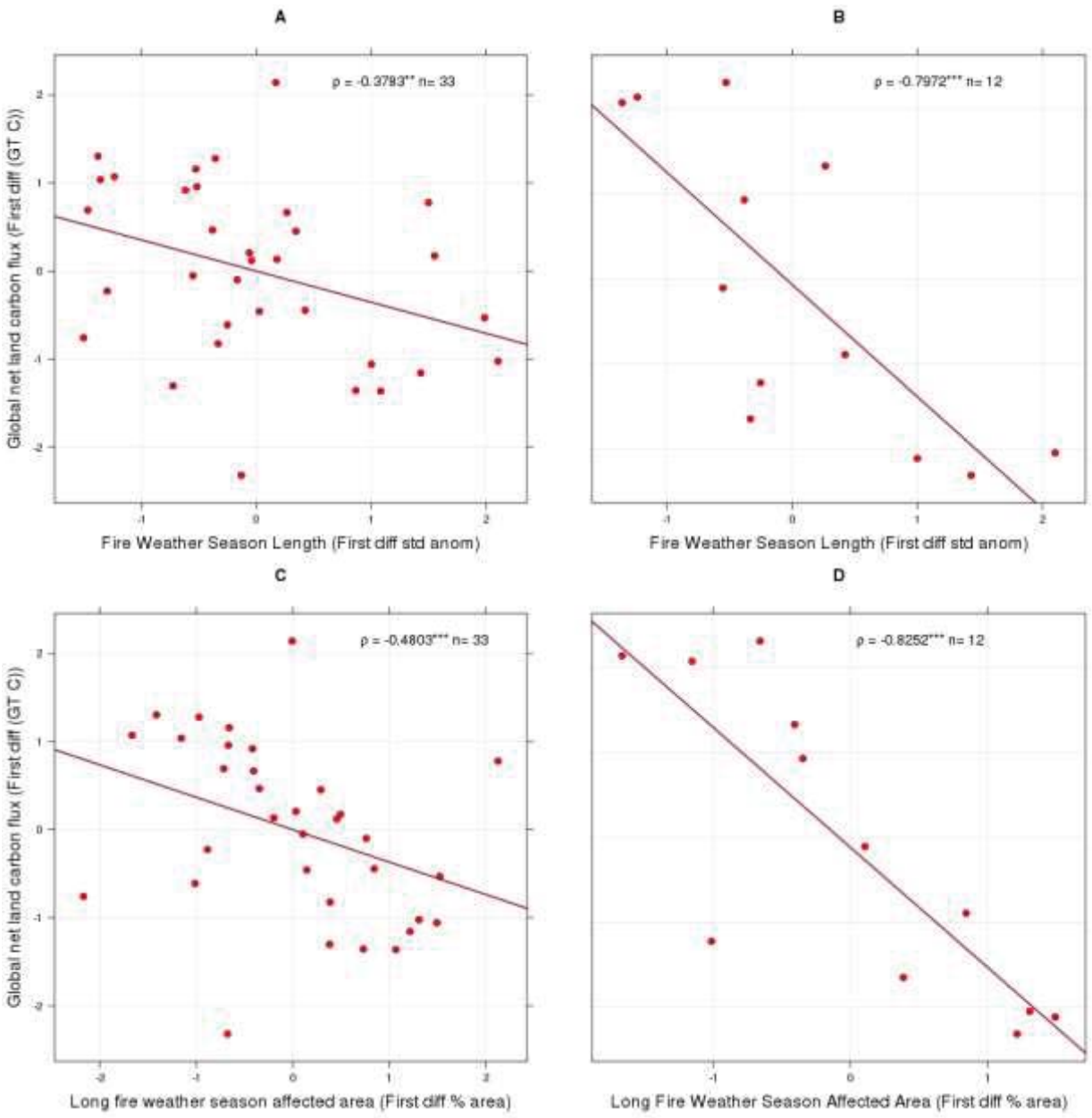

Supplementary Figure 9 – Comparisons of global fire weather season length and long fire weather season affected area to global net land carbon flux from 1979-2012 (A,C respectively) and for the most recent time period where MODIS burned area data were available (2001-2012) (B,D). Values reported in plot upper right are Spearman's rank-order correlation, corresponding significance (* $p < 0.01$, ** $p < 0.05$, * $p < 0.1$, NS Not Significant) and sample size.**

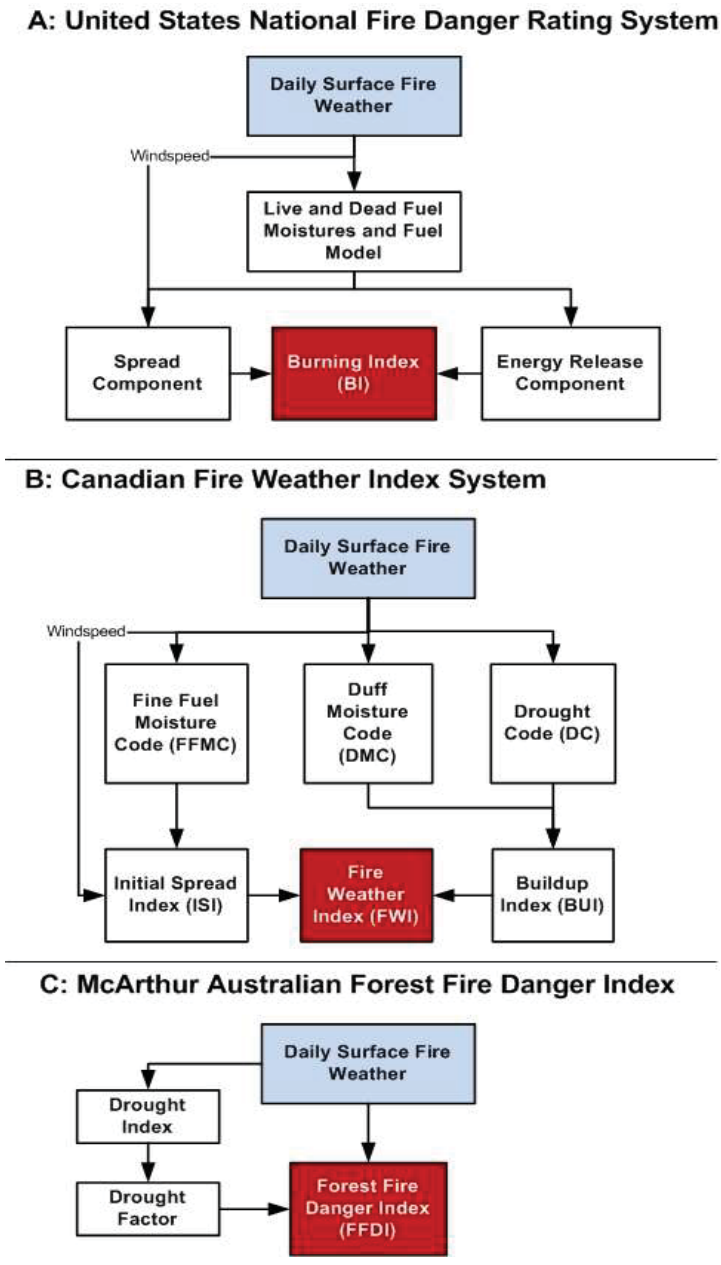

Supplementary Figure 10 – Simplified flow diagram of the US Burning Index (BI), the Canadian Fire Weather Index (FWI) and the Australian Forest Fire Danger Index (FFDI).

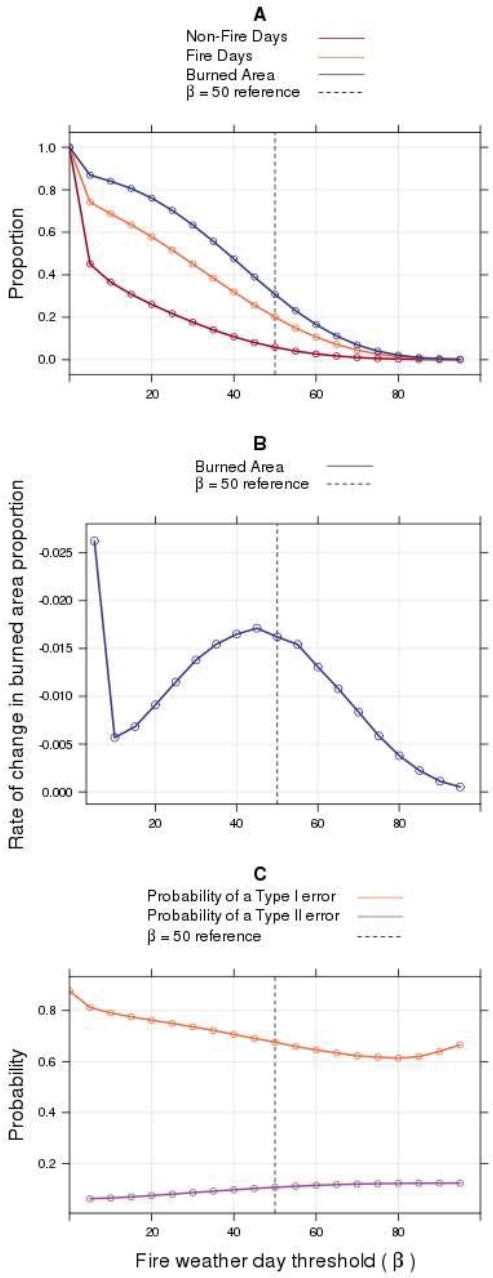

Supplementary Figure 11 – Effect of the selection of β (Equation 2) on the ability of the fire weather day index (FWDI) to capture global fire activity recorded between 2001 and 2012 in the most recent version of the Global Fire Emissions Database (GFED4). The reference value (β=50) was selected *a priori* from literature but these figures show that it represents the best balance between capturing a large portion of the burned area while minimizing the chance of mis-classifying fire days. When β=50, our Fire Weather Day Index captures 20.1% of fire days and 30.8% of the total burned area. Although reducing β captures more fire days and more burned area (A), it also captures an increasing proportion of non-fire days yielding an Ensemble Fire Weather Season Length (EFWSL) that is more representative of days without fire activity. The slope of the curve relating the proportion of burned area to β is steepest near β =50 indicating that reducing the value of β much below 50 captures incrementally smaller gains in total burned area (B). Additionally, reducing β also increases the likelihood making a Type I error (C), where a Fire Weather Day is predicted but no burned area is observed.

Supplementary Tables:

Supplementary Table 1 – Trends in global annual summary meteorological variables and their respective affected area.

Variable	Mean annual value trend		Affected area trend (change in area / yr)	
	Slope	**p-value**	**Slope**	**p-value**
Mean annual maximum temperature (°C)	0.0184°C yr^{-1}	<0.0001	0.628	<0.0001
Mean annual minimum relative humidity (%)	-0.0127% yr^{-1}	0.0356	NS	NS
Mean annual total precipitation (mm)	NS	NS	NS	NS
Mean annual total rain-free period (days)	0.131 days yr^{-1}	0.000985	0.162	0.00162
Mean annual maximum windspeed (km hr^{-1})	0.000691km hr^{-1} yr^{-1}	0.0332	NS	NS

Non-parametric tests examining temporal trends in ensemble-mean global fire weather variables and the area affected by unusual events for mean annual maximum temperature, mean annual minimum relative humidity, total annual precipitation, mean annual rain-free days and maximum 10m windspeed. (NS Not Significant). Slopes were estimated using the Theil-Sen non-parametric trend slope estimator and significance tests were performed using the Mann-Kendall trend test following a four-step approach to reduce the effects of serial autocorrelation on significance tests[1].

Supplementary Table 2 – NCEP Reanalysis and DOE Reanalysis II data variables used to derive fire danger indices.

Variable	Level	Units	Derived Quantity
Maximum temperature	2 m	K	Maximum
Minimum temperature	2 m	K	Minimum
Pressure	Surface	Pa	Mean
Specific Humidity	2 m	kg/kg	Mean
Precipitation Rate	Surface	kg/m2/s	Duration and Total Amount
U/*V* wind	10 m	m/s	Maximum windspeed
Water equivalent of actual snow depth	Surface	kg/m2	Snow flag

Underlying variables used to calculate fire danger indices from both the NCEP Reanalysis and the Reanalysis II datasets. All variables were derived from 4 times daily grids at 192X94 (~2° resolution) Gaussian grid resolution.

Supplementary Table 3 – ECMWF ERA Interim Reanalysis data variables used to derive fire danger indices.

Variable	Level	Units	Summary
Dewpoint temperature	2 m	K	Mean
Air temperature	2 m	K	Maximum / Minimum
Total precipitation	Surface	m	Duration and Total Amount
Snow depth	Surface	m	Snow flag
U/V wind	10 m	m/s	Maximum

Underlying variables used to calculate fire danger indices from the ECMWF Interim Reanalysis. All variables were derived from 8 times daily grids at 479x239 (~0.75° resolution) geographic grid.

Supplementary Table 4 – Summary of classification accuracy of daily MODIS burned area based on daily Fire Weather Day Indices.

Beta	Type I Error (False Positive)	Correct Decision (True Positive)	Correct Decision (True Negative)	Type II Error (False Negative)
	Conditional Probability of **No** MODIS BA detection given a Fire Weather Day	Conditional Probability of a MODIS BA detection given a Fire Weather Day	Conditional Probability of **No** MODIS BA detection given a Non-Fire Weather Day	Conditional Probability of a MODIS BA detection given a Non-Fire Weather Day
β	**Pr(BA=0|FWDI=1)**	**Pr(BA>0|FWDI=1)**	**Pr(BA=0|FWDI=0)**	**Pr(BA>0|FWDI=0)**
0	0.88	0.12	Undefined	Undefined
5	0.81	0.19	0.94	0.06
10	0.79	0.21	0.94	0.06
15	0.78	0.22	0.93	0.07
20	0.76	0.24	0.93	0.07
25	0.75	0.25	0.92	0.08
30	0.74	0.26	0.91	0.09
35	0.72	0.28	0.91	0.09
40	0.71	0.29	0.90	0.10
45	0.69	0.31	0.90	0.10
50	0.68	0.32	0.89	0.11
55	0.66	0.34	0.89	0.11
60	0.65	0.35	0.89	0.11
65	0.63	0.37	0.88	0.12
70	0.62	0.38	0.88	0.12
75	0.62	0.38	0.88	0.12
80	0.61	0.39	0.88	0.12
85	0.62	0.38	0.88	0.12
90	0.64	0.36	0.88	0.12
95	0.67	0.33	0.88	0.12

Contingency table values of the ability of the Fire Weather Day Index to accurately classify the probability of a MODIS burned area day.

Supplementary Methods:

Wildfire Danger Indices

Global reanalysis data, summarized to daily values , were input into three common wildland fire danger rating systems: The United States National Fire Danger Rating System (USNFDRS), the Canadian Fire Weather Index System (CFWIS) and the McArthur Forest Fire Danger Index (FFDI).

A single C++ based library was created that allows the simultaneous calculation all fire danger indices. The USNFDRS library is the same library used operationally to assess fire danger for all fire management applications. All USNFDRS fuel moistures, components and indices were computed following Bradshaw et al.[2]. To ensure that indices were comparable spatially and temporally and to allow the combination of US indices with other indices, we constrained all calculations to Fuel Model G as recommended by Andrews[3]. This fuel model heavily weights long time-lag fuels, such as 100 hour and 1000 hour classes, and thus best represents seasonal wetting and drying cycles[3]. The USNFDRS culminates in a single index, called the Burning Index (BI), that is related to both the expected rate of spread and heat release of an initiating fire. The US Burning Index is calculated by combining meteorological variables to first calculate time-lag fuel moisture contents. Fuel moisture contents are then combined to calculate the Spread Component and the Energy Release Component which were then used to calculate the Burning Index (Supplementary Figure 10A).

The Canadian Forest Fire Weather Index (FWI) was computed following Van Wagner and Pickett[4], with variable latitude adjustment factors to allow these indices to be calculated globally[5]. Similar to the US system, Canadian FWI are aligned as a two-step process. First, three "Codes" are calculated using surface weather data and then these codes are combined into "Indices". Surface weather was used to calculate the Fine Fuel Moisture Code, the Duff Moisture Code and the Drought Code and these Codes were combined to calculate the Initial Spread Index (ISI) and the Build-up Index (BUI). Finally, the ISI and BUI are combined to calculate the Fire Weather Index (Supplementary Figure 10B). Generally, both the US and Canadian systems are applied using afternoon weather (either 1200 or 1300 local standard time) but to ensure global applicability, all calculations were performed substituting daily maximum temperature and minimum relative humidity for midday weather. Further, in areas with ephemeral snow cover, both the US and Canadian indices were initialized to start-up values each season anytime snow cover was present. For consistency between indices, the

effects of prolonged drought, typically accounted for by 'overwintering' the Drought Code, were ignored[6].

The McArthur (Australian) Forest Fire Danger Index (FFDI) was calculated following the logic presented by McArthur and expressed as equations by Noble[7]. The Drought Factor for these equations was calculated using the improved formula presented by Griffiths[8] driven by the Keetch-Byram Drought Index (Supplementary Figure 10C). KBDI was calculated using daily maximum temperature and precipitation from each reanalysis dataset and mean annual precipitation values from the WorldClim climate dataset[9]. The BI, FWI, and FFDI were each calculated using the NCEP Reanalysis, the NCEP DOE Reanalysis II and the ECWMF Interim Reanalysis data to yield nine independent daily fire danger indices at 0.75°×0.75° spatial resolution for the ECWMF and an approximately 2° × 2° spatial resolution for the NCEP and NCEP DOE Reanalysis II datasets.

Developing metrics of wildfire weather season length

While some systems, such as the Canadian Fire Weather Index System, have established thresholds for its indices that relate to periods where fires spread actively[10, 11], the other two systems have no similar thresholds. Therefore, a common way of normalizing and comparing all three indices across space and time is needed. The magnitudes of each of the three BI, FWI, and FFDI indices vary spatially and temporally, by up to two orders of magnitude, making it necessary to normalize each daily index relative to its historical range for that location. An established practice is to normalize each daily value based on the historical maximum and minimum recorded in the grid cell[12]. This procedure ensures that time-series of fire danger indices can be compared between re-analysis projects and between grid cells across the globe. Daily fire danger indices were normalized in each grid cell as follows:

$$FDI_{Norm_{ij}} = \left[\frac{FDI_{ij} - FDI_{Min}}{FDI_{Max} - FDI_{Min}}\right] * 100 \qquad \text{Equation 1}$$

Where FDI_{ij} is the daily fire danger index for a given location for day i of year j, FDI_{Min} and FDI_{Max} are the historical daily minimum and maximum fire danger indices for that location for the entire time series, and FDI_{Normij} is the normalized, daily fire danger index. FDI_{Normij} is bounded by 0 and 100 indicating the historical minimum and maximum fire danger index for each grid cell, respectively.

Fire Weather Days

Once normalized, we expressed each day as either a fire weather day or a non-fire weather day as follows:

$$FWDI_{ij} = \begin{cases} 1: FDI_{Norm_{ij}} \geq \beta \\ 0: FDI_{Norm_{ij}} < \beta \end{cases} \qquad \text{Equation 2}$$

Where FDI_{Normij} is the daily, normalized fire danger index calculated from Equation 1 and $FWDI_{ij}$ is a fire weather day index indicating that wildfire potential exceeded the threshold β on a particular day. Setting the threshold of β = 0 implies that all days are fire weather days, and increasing the value of β corresponds to more conducive fire weather conditions. For our analysis, we set β=50 *a priori* based on the established technique commonly used to identify phenological events such as leaf out and leaf senescence using satellite time series of vegetation indices[13]. A universal threshold of β=50 lies at the midpoint between the lower and upper values recorded over the entire time-series in each grid cell, and as such, standardizes the comparison of fire weather across space and time.

We evaluated our *a priori* choice of β to assess the ability of the fire weather day index to capture daily fire activity by associating the normalized daily fire danger index (FDI_{Normij}) with the daily burned area recorded in the most recent version of Global Fire Emissions Database (GFED4)[14]. GFED4 summarizes the daily 500m Collection 5.1 MODIS direct broadcast (DB) burned area product (MCD64A1) at 0.25° spatial resolution (since August 2000)[15]. We used 11 years of daily

data (2001 to 2012) resampled to the gridded domain of FDI_{Norm}. Synchronizing fire danger and fire activity in each grid cell yielded 9 daily time series of FDI_{Norm} (one for each fire danger index and reanalysis data combination) and a daily time series of burned area. We varied the β threshold in 1 Equation 2 that is used to determine the Fire Weather Day Index and we quantified the mean proportion of fire days (i.e., a day with at least one 500m burned area pixel in a grid cell), mean proportion of non-fire days and the mean proportion of burned area captured by the 9 values of the 4 FWDI (Supplementary Figure 11A).

Results indicate that our *a priori* selection of β=50 captures 20.1% of fire days and 30.8% of the total global burned area. Additionally, it aligns closely with the point of maximum rate of change of captured burned (Supplementary Figure 11A), thus the FWDI captures smaller gains in burned area as the threshold β varies both above and below β=~45 (Supplementary Figure 11B). Although reducing β necessarily captures more fire days and more burned area (Supplementary Figure 11A), selecting a lower β threshold leads to a higher probability of making a Type I error, where we classify a fire weather day but MODIS does not detect burned area on that day (Supplementary Figure 11C and Supplementary Table 4). Conversely, increasing β above 50 to 80 minimizes the Type I errors (Supplementary Table 5) but it only captures 1.4% of the global fire days and 2.2% of the burned area (Supplementary Figure 11A). Despite being selected *a priori*, our choice of β=50 is the best compromise between minimizing the probability of a Type I error while maximizing the burned area captured by our Fire Weather Day Index. Finally, our index is based only on fire weather; it does not incorporate any information about available fuels or sources of ignition. While we expect that if ignited, a fire will spread more rapidly on a fire weather day, we do not expect to explain all the variations in global burned area with weather alone, especially given that human-ignited fires burning outside the seasonal peak of fire weather account for a large proportion of the annual global burned area[16].

Ensemble Fire Weather Season Length

Whilst the same logic is commonly used to determine growing season length from satellite-derived vegetation indices[13, 17], our goal is to estimate a fire weather season length. We calculate an annual "Fire Weather Season Length" that represents the number of days (not necessarily continuous) during each calendar year at a given location that observed high fire danger and thus experienced weather conditions most conducive to ignition and burning, as follows:

$$\boldsymbol{FWSL_j = \sum_{i=1}^{365|366} FWDI_{ij}} \qquad \textbf{Equation 3}$$

Where $FWDI_{ij}$ is the daily fire weather day index calculated from Equation 2 and $FWSL_j$ is the annual Fire Weather Season Length (FWSL) in days for year j. FWSL is calculated in each grid cell for each fire danger index (BI, FWI, FFDI) and reanalysis dataset (NCEP, NCEP II and ECMWF Interim), yielding nine annual fire weather season length values for each grid cell. Because climate studies using multi-model ensembles are generally superior to single model approaches[18], an ensemble-mean fire weather season length is calculated as follows:

$$\boldsymbol{EFWSL_j = \frac{\sum_{n=1}^{9} FWSL_{jn}}{9}} \qquad \textbf{Equation 4}$$

Where $FWSL_j$ is the FWSL calculated for a given location and a given index / model combination (n) and $EFWSL_j$ is the Ensemble-mean Fire Weather Season Length across all nine index / model combinations in a grid cell for year j.

To allow combination of disparate raster resolutions into a single ensemble dataset, the coarse fire weather season length raster datasets derived from BI, FWI and FFDI using the NCEP and NCEP II datasets were resampled to match the 0.75° x 0.75° resolution of the ECMWF Interim Reanalysis dataset using the nearest neighbor method. After resampling, all nine fire weather season length

raster datasets were averaged for each year from 1979 to 2013 to produce an Ensemble Fire Weather Season Length raster dataset at 0.75° x 0.75° resolution (Equation 4).

We also calculated a standardized anomaly by expressing the annual $EFWSL_j$ in each grid cell relative to its 35-year mean and standard deviation as follows:

$$EFWSL_{Anom_j} = \frac{EFWSL_j - \overline{EFWSL}}{\sigma EFWSL} \qquad \text{Equation 5}$$

Where $EFWSL_j$ is the annual ensemble mean fire weather season length calculated above, $\overline{EFWSL}$ and $\sigma EFWSL$ are the 35 year mean and standard deviation of EFWSL for that location and $EFWSL_{Anomj}$ is the standardized anomaly of EFWSL for year j for a given location. All analyses are performed on either the ensemble fire weather season length or its anomalies. For simplicity, the term "Fire Weather Season Length" is used throughout to denote the Ensemble Fire Weather Season Length.

Analysis

We used a simple mask that delineated vegetated and non-vegetated areas that was developed approximately in the middle of the study period[19]. Pixels were considered vegetated if they were not listed as: water, bare ground or urban and built-up in the land cover dataset. All spatial mean trends were calculated using a cell-area-weighted average because the cell sizes of the geographic projection that we used for the dataset vary from the equator to the pole. Trend significance was evaluated using the Mann-Kendall trend tests[20] by following a four-step trend-free prewhitening (MKTFPW) approach that reduces the impact of serial autocorrelation on significance tests[1]. Trend slopes were estimated using the non-parametric Theil-Sen (TS) trend estimator[21, 22]. Further, pixel-based trend analyses were performed using the MKTFPW and the TS trend slope estimator and all pixels with significant fire weather season length trends ($p < 0.05$) were mapped to produce Figure 3A. Because climatic changes can lead to either a persistent trend or an increase in rare events, we

also examined the changes in the global frequency of long fire weather seasons. A long fire weather season was defined as any year where a given pixel's fire weather season length was more than 1 standard deviation above the mean. We then summed the total land area of all vegetated pixels that experienced these unusually long fire weather seasons each year. Hereafter, this metric is referred to as: long fire weather season affected area. We plotted these global affected area sums over time from 1979 to 2013 (Figure 2B). Finally, we developed a simple way to spatially depict areas that have witnessed changes in the frequency of these long fire seasons. For each pixel, we determined the number of times that fire weather season length standard anomalies exceeded one standard deviation from the mean. Hereafter, any year with an anomalous fire season length will be termed an event 5 year. We then summed the number of events from 1979-1996 (18 years) and we summed the number of events from 1996-2013 (18 years), where 1996 overlaps to yield the same number of years in each period. We mapped the difference between the number of events in the second period and the number of events in the first period and expressed that difference as a percentage change in the number of years (Figure 3B).

Comparison to country-wide reported burned area

To determine the degree to which the fire weather season length is related to observed fire activity, we compared yearly spatial-mean fire weather season length values to published total annual area burned on US federal lands, documented by the National Interagency Fire Center (NIFC)[23], area burned across Canadian Forests[24] and for six European countries (Spain, Portugal, France, Italy, Greece and Latvia), where annual burned area reports were available from 1980-2013. Two comparisons were made for the United States. We first compared mean fire weather season length across the United States (including Alaska) to annual burned area from 1992-2013. Fire occurrence data prior to 1992 are often incomplete and thus reported burned area may or may not accurately reflect actual burned area[25]. However, because burned area estimates are published by the National

Interagency Fire Center for our entire study period, we also compared mean fire weather season length to burned area for the full period, with the caveat that data prior to 1992 may be somewhat incomplete. We compared mean annual fire weather season length and long fire weather season affected area for each country to their reported burned area. All time series were first-difference detrended to ensure stationarity and all comparisons were performed using the Spearman's rank-order correlation. Correlations are reported in Table 4 and plots of all comparisons are shown in (Supplementary Figure 5-8).

Regional fire weather season length trends

Global patterns in fire weather season length were further constrained to examine changes across continents and biomes. A coarse-level biome map was derived from the World Wildlife Fund (WWF) Ecoregions biome classification[26]. Since the spatial resolution of the climate datasets was coarser than some of the biome delineations, we aggregated multiple WWF biomes into eight broad biome classes (See Supplementary Table 5). The same methods used to assess the global trends (defined above) were also used to assess (i) continental, (ii) biome, and (iii) continental × biome trends. Continental boundaries were used to develop an analysis map, excluding Antarctica and combining Europe and Asia, as well as Australia and New Zealand. The continental and biome analysis maps were used to assess changes in continental average (Table 1), global biome average (Table 2), and continent × biome average fire weather season length as well as long fire weather season affected area (Table 3). Finally, five number summaries (minimum, first quartile, median, third quartile and maximum) were generated for all pixels that fall within each continent x biome combination that had significant trends in fire weather season length to assess central tendencies and range of fire weather season length changes (Table 6).

Comparisons to global carbon fluxes

To assess the degree to which fire weather season lengths are potentially coupled to global carbon emissions, we compared the mean global fire weather season length and the long fire weather season

affected area to the global annual net land carbon uptake computed from the Global Carbon Budget dataset from 1979-2012[27]. This carbon budget decomposes global annual carbon fluxes and a global annual carbon 'land sink' is computed as follows:

$$LndSnk = FF\text{-}CPE + LUCE - AtmGr - OcnSnk \quad \text{Equation 6}$$

Where *LndSnk* is the land carbon sink, *FF-CPE* are fossil fuel and cement production emissions[28], *LUCE* is land-use change emissions[29], *AtmGr* is the atmospheric CO_2 growth rate and *OcnSnk* is the ocean carbon sink[27]. All global fluxes are reported in billions of tons of carbon per year (GtC per yr). Because we were interested in comparing our global fire weather season length metric to variations in global land carbon flux variations, which includes components of the global land sink as well as components of land-use change emissions, we computed a global net land carbon flux as follows:

$$NetLndCFlux = LndSnk - LUCE \quad \text{Equation 7}$$

Where *NetLndCFlux* is the global net land carbon flux and *LndSnk* and *LUCE* are explained above. This metric is positive when there is a net carbon uptake by the land surface and negative when there is a net loss of terrestrial carbon. It accounts for potential variations in land-use change emissions as well as other potential wildfire-derived carbon emissions that are not a direct result of land-use change activities but that are embedded in the total global land carbon flux. Two comparisons were performed: one for the entire available, overlapping time series (1979-2012), and another where correlations were constrained to the time period that satellite burned area observations were available from the Moderate Resolution Imaging Spectroradiometer (MODIS) (2001-2012), and thus when estimates of land-use change carbon emissions were more certain[14]. All time series were first-difference detrended to ensure stationarity and all comparisons

were performed using the Spearman's rank-order correlation. Correlations were also examined between continent x biome-mean fire weather season length, long fire season affected area and global net land carbon flux to assess where fire might be most coupled to the global carbon cycle.

Supplementary References:

1. Yue S, Pilon P, Phinney B, Cavadias G. The influence of autocorrelation on the ability to detect trend in hydrological series. *Hydrological Processes* **16**, 1807-1829 (2002).

1. Yue S, Pilon P, Phinney B, Cavadias G. The influence of autocorrelation on the ability to detect trend in hydrological series. *Hydrological Processes* **16**, 1807-1829 (2002).

2. Bradshaw LS, Deeming JE, Burgan RE, Cohen JD. The 1978 NFDRS: technical documentation. *USDA Forest Service, Gen Tech Rep INT-169*, (1983).

3. Andrews PL, Loftsgaarden DO, Bradshaw LS. Evaluation of fire danger rating indexes using logistic regression and percentile analysis. *International Journal of Wildland Fire* **12**, 213-226 (2003).

4. Van Wagner CE, Pickett TL. *Equations and FORTRAN program for the Canadian forest fire weather index system*. Canadian Forestry Service (1985).

5. Lawson BD, Armitage OB. *Weather guide for the Canadian forest fire danger rating system*. Northern Forestry Centre (2008).

6. Turner JA, Lawson BD. Weather in the Canadian forest fire danger rating system. A user guide to national standards and practices. *Report Pacific Forest Research Centre*, (1978).

7. Noble IR, Gill AM, Bary GAV. McArthur's fire-danger meters expressed as equations. *Australian Journal of Ecology* **5**, 201-203 (1980).

8. Griffiths D. Improved Formula for the Drought Factor in McArthur's Forest Fire Danger Meter. *Australian forestry* **62**, 202-206 (1999).

9. Hijmans RJ, Cameron SE, Parra JL, Jones PG, Jarvis A. Very high resolution interpolated climate surfaces for global land areas. *International Journal of Climatology* **25**, 1965-1978 (2005).

10. Podur J, Wotton BM. Defining fire spread event days for fire-growth modelling. *International Journal of Wildland Fire* **20**, 497-507 (2011).

11. Wang X*, et al.* The potential and realized spread of wildfires across Canada. *Global Change Biology*, (2014).

12. Viegas DX, Bovio G, Ferreira A, Nosenzo A, Sol B. Comparative study of various methods of fire danger evaluation in southern Europe. *International Journal of Wildland Fire* **9**, 235-246 (1999).

13. White MA, Thornton PE, Running SW. A continental phenology model for monitoring vegetation responses to interannual climatic variability. *Global Biogeochemical Cycles* **11**, 217-234 (1997).

14. Giglio L, Randerson JT, van der Werf GR. Analysis of daily, monthly, and annual burned area using the fourth generation global fire emissions database (GFED4). *Journal of Geophysical Research: Biogeosciences* **118**, 317-328 (2013).

15. Giglio L, Loboda T, Roy DP, Quayle B, Justice CO. An active-fire based burned area mapping algorithm for the MODIS sensor. *Remote Sensing of Environment* **113**, 408-420 (2009).

16. Le Page Y, Oom D, Silva JMN, Josson P, Pereira JMC. *Global Ecology and Biogeography* **19**, 575-588 (Seasonality of vegetation fires as modified by human action: observing the deviation from eco-climatic fire regimes).

17. de Beurs KM, Henebry GM. Spatio-temporal statistical methods for modelling land surface phenology. In: *Phenological research* (ed^(eds). Springer (2010).

18. Hagedorn R, Doblas-Reyes FJ, Palmer TN. The rationale behind the success of multiâ€• model ensembles in seasonal forecasting--I. Basic concept. *Tellus A* **57**, 219-233 (2005).

19. Hansen MR, DeFries RS, Townshend JRG, Sohlberg R. Global land cover classification at 1km resolution using a decision tree classifier. *International Journal of Remote Sensing* **21**, 1331-1365 (2000).

20. Mann HB. Nonparametric tests against trend. *Econometrica: Journal of the Econometric Society*, 245-259 (1945).

21. Sen PK. Estimates of the regression coefficient based on Kendall's tau. *Journal of the American Statistical Association* **63**, 1379-1389 (1968).

22. Thiel H. A rank-invariant method of linear and polynomial regression analysis, Part 3. In: *Proceedings of Koninalijke Nederlandse Akademie van Weinenschatpen A* (ed^(eds) (1950).

23. National Interagency Fire Center. Total Wildland Fires and Acres (1960-2013), 7 <http://www.nifc.gov/fireInfo/fireInfo_stats_totalFires.html> (2014).

24. Canadian National Forestry Database. Forest Fire Statistics by Province/Territory/Agency, 1970-2013, <http://nfdp.ccfm.org/data/compendium/html/comp_31e.html> (2014).

25. Short K. A spatial database of wildfires in the United States, 1992-2011. *Earth System Science Data* **6**, 1-27 (2014).

26. Olson DM, Dinerstein E, Wikramanayake ED, Burgess ND, et al. Terrestrial ecoregions of the world: A new map of life on Earth. *Bioscience* **51**, 933-938 (2001).

27. Le Quéré C*, et al.* Global carbon budget 2013. *Earth Syst Sci Data* **6**, 235-263 (2014).

28. Boden TA, Marland G, Andres RJ. Global, regional, and national fossil-fuel CO_2 emissions. *Carbon Dioxide Information Analysis Center, Oak Ridge National Laboratory, US Department of Energy, Oak Ridge, Tenn, USA doi* **10**, (2009).

29. Houghton RA, *et al.* Carbon emissions from land use and land-cover change. *Biogeosciences* **9**, 5125-5142 (2012).